OPTICAL AND ELECTRICAL PROPERTIES OF DILUTE GaN$_x$As$_{1-x}$ ALLOYS

by

Eric Strohm

B.Sc McMaster University 1999

A dissertation submitted in partial satisfaction of the
requirements for the degree of
MASTER OF SCIENCE

in

THE FACULTY OF GRADUATE STUDIES
Department of Physics and Astronomy

We accept this thesis as conforming
to the required standard

UNIVERSITY of BRITISH COLUMBIA
2002

Department of _Physics and Astronomy_

The University of British Columbia
Vancouver, Canada

Date _Jan 8, 2002_

Abstract

The bandgap and optical absorption edge are measured in semi-insulating and p-type GaNAs as a function of nitrogen content using a photoconductivity technique. The bandgap is found to decrease from 1.42 eV with 0% nitrogen to 1.20 eV with 0.9% nitrogen, and to 1.14 eV with 1.73% nitrogen content. The characteristic energy of the exponential absorption edge (Urbach parameter) for p-type GaNAs is found to increase from 6.7 meV with 0% nitrogen to 14 meV with 0.8% nitrogen content.

The mobility and carrier concentration are measured as a function of nitrogen content in p-type and n-type GaNAs using Hall measurements. The electron mobility decreases from 3000 cm^2/Vs with 0% nitrogen, to 650 cm^2/Vs with 0.1% nitrogen, and to 300 cm^2/Vs with 1.0% nitrogen content. The hole mobility is relatively unaffected by nitrogen and stays constant around 300 cm^2/Vs for up to 1% nitrogen content. The carrier concentration in p-type GaNAs is found to decrease for highly doped (2.5x10^{16} cm^{-3}) GaNAs and increase for low doped (4.5x10^{14} cm^{-3}) GaNAs with increasing nitrogen content. The carrier concentration converges to 7x10^{15} cm^{-3} for both low and high doping at greater than 0.8% nitrogen content, which suggests there is a trap that is pinning the Fermi level. This behaviour is modeled using conservation of charge in the band gap, and a

trap level at 0.18 eV above the top of the valence band is found to explain the experimental data.

A new method for measuring the bandgap and Urbach edge in epitaxial semiconductor films using photoconductivity is presented. In this method the sample is illuminated with monochromatic light, and the photoconductivity is measured as a function of incident wavelength. Light with energy greater than the band gap is absorbed by the sample and increases the photoconductivity signal. The absorption coefficient is determined from the photoconductivity signal. The electrical properties, such as the mobility and carrier concetration are obtained from Hall measurements.

Contents

List of Tables

List of Figures

Acknowledgements

I would like to thank my supervisor Tom Tiedje for his support in this research. His incredible insight and intuition into physics problems never ceased to amaze me.

I would specifically like to thank Martin Adamcyk, who grew all my samples and took countless hours out of his busy schedule to help with my research. Other people I could always count on for their help in the lab are Anders Ballestad, Eric Nodwell, Arman Rahmim, Ben Ruck, Jens Schmid, Sebastien Tixier, Mya Warren and Mike Whitwhick. Thanks guys for a great time. I could not have finished this thesis without the help of Jim MacKenzie and Al Schmalz, who were kept busy fixing everything we broke.

Finally, thank you to my mom, dad and my sister, Elaine, whose support over the past few years has been invaluble to me.

Chapter 1

Introduction

Compound semiconductor III-V nitride alloys (such as GaNAs and InGaNAs) have unique physical properties and have emerged as a subject of recent theoretical and experimental interest. Incorporation of small amounts of nitrogen into GaAs and InGaAs dramatically reduce the measured bandgap. This allows for the production of long-wavelength (1.3 - 1.55 μm) devices on GaAs substrates for optical fibre communications, which have many advantages over current materials used, such as InGaAsP/InP or InGaAs/InGaAsP[1]. Lasers made from InGaNAs alloys are less temperature dependent due to the larger conduction band offset[2]. A higher temperature stability is desirable for uncooled lasers for use in optical fibre communications. Devices based on GaNAs/GaAs alloys are easier to fabricate than current devices, and GaAs substrates have a lower cost than InP which allows for lower cost device manufacturing.

One disadvantage to nitride materials is that they show poor electrical and optical characteristics. Also a large decrease in the electron mobility, a decrease in the recom-

bination lifetime and a reduction in the photoluminescence efficiency have been reported. GaNAs has a smaller lattice constant than GaAs due to the smaller size of the nitrogen atoms. When GaNAs is grown on GaAs substrates, strain is created in the GaNAs epi-layer due to the lattice constant mismatch. Alloying with both In and N allows for 1.3 μm and 1.55 μm lasers to be grown lattice-matched to GaAs. InGaNAs shows similar electrical properties to GaNAs, such as a decrease in the electron mobility with nitrogen content and additional recombination centers.

1.1 Background

1.1.1 Band Gap Bowing

The bandgap and lattice constant of semiconductors change as the composition of an alloy is modified. For example, increasing the amount of Al in GaAs from 0% to 100% (effectively displacing all the Ga atoms to create AlAs) increases both the bandgap and lattice constant; since alloys are generally grown lattice-matched to their substrate, it is important to know how the bandgap shifts as a function of lattice constant. The change in bandgap as a function of lattice constant for common semiconductor compounds is shown in Figure 1.1.

The variation in the bandgap for GaNAs alloys can be estimated using a simple parabolic law[3]

$$E_G(GaN_xAs_{1-x}) = xE_G(GaN) + (1-x)E_G(GaAs) - bx(x-1) \qquad (1.1)$$

where b is the bowing coefficient, $E_G(GaN) = 3.4$ eV, and $E_G(GaAs) = 1.412$ eV. The

bowing coefficient is typically just a fraction of an eV for many binary and ternary alloys,

however GaNAs has an unusually large bowing parameter which has been measured to be

-19 eV[4], which results in a dramatic change in the bandgap of GaAs and GaN, as indicated

by the dotted line in Figure 1.1. Note that the bandgap of GaNAs has been calculated to

be negative for certain nitrogen compositions, and therefore should behave like a metal in

this region.
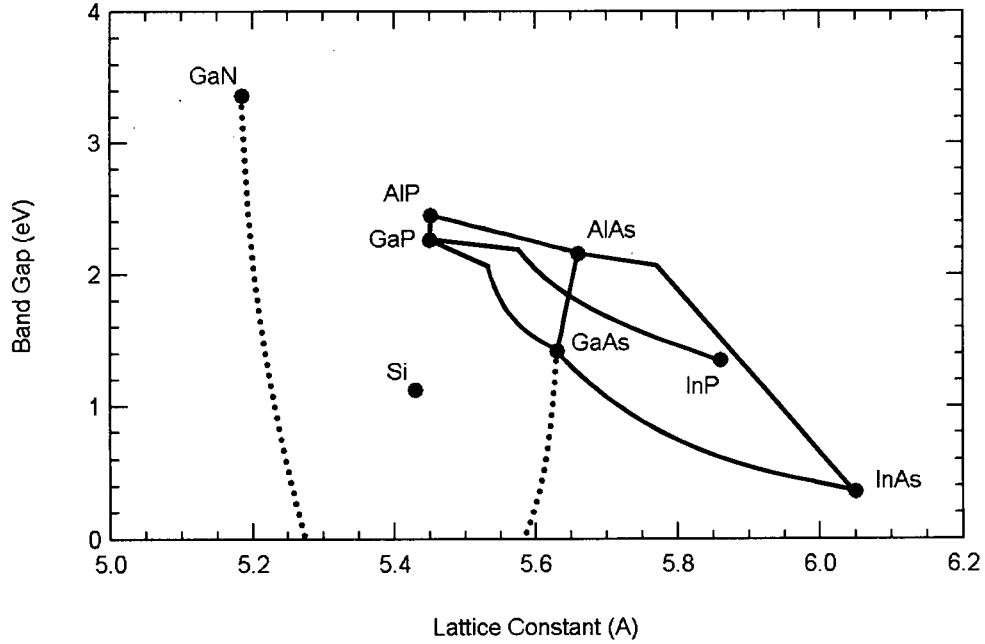
Figure 1.1: Band gap bowing of common semiconductors. GaNAs is the dotted line.

1.1.2 Levels Due to Nitrogen Incorporation

· It has been experimentally shown that nitrogen in GaAs creates a resonant state

about 0.2 eV above the conduction band minimum[5]. The nitrogen resonant state tends

to flatten out the bottom of the conduction band, which may result in a higher conduction band effective mass for nitride alloys[6]. Calculations show that nitrogen substitution for As in GaAs induces intraband coupling with the nitrogen resonance level and the conduction band[7]. This intraband coupling causes intraband level repulsion which decreases the conduction band minimum[8]. The valence band is relatively unaffected by nitrogen, as the valence band offset has been experimentally shown to be only 11 meV above the GaAs valence band with 3% nitrogen, compared to a conduction band offset of over 200 meV[9].

An increased number of traps and deep levels have been observed in GaNAs and InGaNAs compared with GaAs or InGaAs. Nitrogen on Ga or As sites induce impurity-like empty levels in the bandgap, which act as acceptors as discussed in reference [10].

1.2   Methods of Investigation

Nitride alloys have several unresolved physics problems, such as how nitrogen affects the transport properties and the reason for the an increase in the number of traps over GaAs. This thesis attempts to bring answers to some of these questions by using several methods to measure the electronic and optical properties of nitride alloys. Photoconductivity measurements are used to obtain the bandgap, density of deep levels and the Urbach parameter, which is a measure of the amount of disorder in the alloy. Hall and resistivity measurements are used to measure carrier concentration and mobility of carriers in the alloys.

Chapter 2

Sample Growth and Preparation

2.1 Sample Growth

The samples studied in this thesis were grown by molecular beam epitaxy (MBE) in an ultra-high vacuum (UHV) environment onto semi-insulating GaAs wafers. A GaAs buffer layer 300 nm thick was deposited onto the substrate first, then a GaNAs layer was grown on top. Figure 2.1 shows the layered growth cross-section of the resulting sample. A RF nitrogen plasma source was used to incorporate nitrogen into the GaAs alloy during growth. The GaNAs samples ranged in thickness from 0.2 to 0.6 μm, 0.3 μm being typical. Silicon was used to dope the alloys n-type, and beryllium was used for p-type doping.

The arsenic and gallium fluxes remained constant for the growth of the samples examined in this thesis. As_2 was used with a beam equivalent pressure (BEP) of approximately 3.3×10^{-6} mBar. The As/Ga ratio was slightly greater than one, and a solid 2x4 reconstruction was maintained. The nitrogen source parameters remained constant for all sample growths, only the nitrogen pressure was varied to change the nitrogen flux. The

substrate temperature varied between 460°C to 500°C during growth.

GaNAs	300 nm
GaAs buffer layer	300 nm
GaAs semi-insulating substrate	350 μm

Figure 2.1: Cross-section of a GaNAs sample. An undoped GaAs layer is deposited onto a GaAs semi-insulating wafer, onto which the GaNAs top layer is then grown.

The nitrogen content in these samples ranged from 0% to just under 2%. It is possible to grow samples with greater than 2% nitrogen content, but the larger lattice size of the GaAs substrate induces strain in the GaNAs layer, which increases as the nitrogen content increases. If the sample thickness exceeds a critical value, cracks and dislocations form, which are detrimental to the electrical and optical properties. The larger the strain, the thinner the sample has to be to prevent the formation of cracks and dislocations[11].

2.2 Nitrogen Incorporation in GaAs

Nitrogen gas does not incorporate into the samples during MBE growth. It must first be dissociated into reactive species, such as atomic nitrogen (N) or excited nitrogen (N_2^*). This is accomplished by using a helical resonator which creates a nitrogen plasma whose output is directed at the sample during growth. The plasma source consists of a copper coil, a wire tap to supply power to the coil from outside of the UHV flange and a pyrolytic boron nitride (PBN) tube for the nitrogen gas. A grounded cylindrical metal shield covers the coil during operation. A baffle is used at the end of the PBN tube to suppress the

high energy ions emitted from the source, which possibly damage the film. A schematic of the plasma source is shown in Figure 2.2. One end of the coil is grounded and the other end is an open circuit. RF power is fed to the coil through a wire tap located part way along the coil. The coil has distributed inductance and capacitance, and RF resonance is achieved by this L-C parallel circuit[12]. The impedance of the plasma source is typically different from that of the power source, and a considerable amount of power is reflected from the plasma. Ideally the RF generator output impedance and the helical resonator impedance with the plasma ignited should be equal so that no power is reflected. A matching network is commonly used to achieve this in conventional plasma discharge sources, however in our helical resonator the input impedance can be adjusted by the position of the wire tap and the operating frequency to achieve zero reflected power[13].
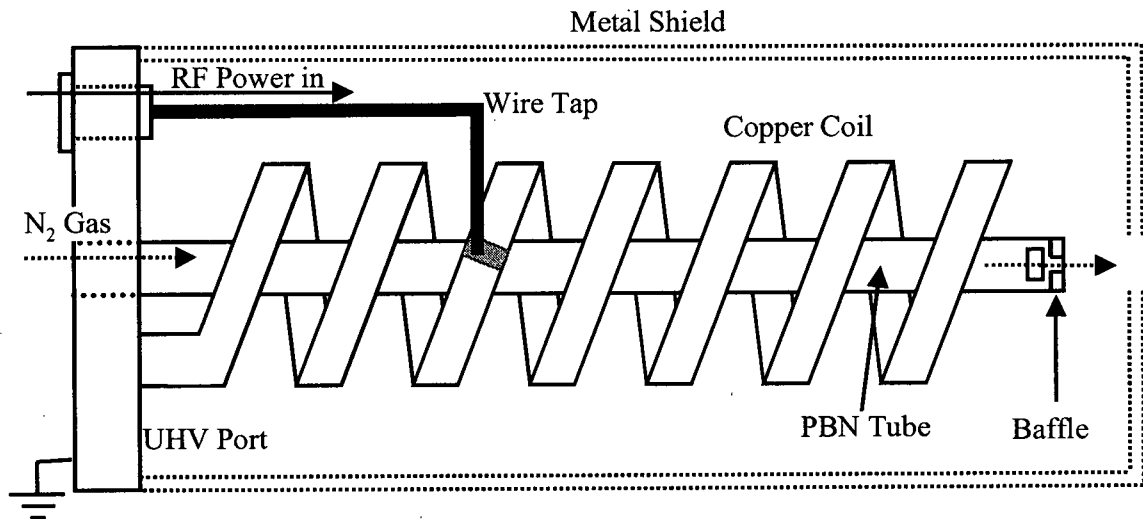
Figure 2.2: Design of the RF nitrogen plasma source. Power is applied to the copper coil through a wire tap, which ignites the nitrogen gas flowing through the tube into a plasma.

2.3   Design of the RF Plasma Source

The design of the plasma source was based on a paper by Macalpine *et al.*[14], detailing optimum conditions for a helical resonator. Resonance frequencies for various positions of the wire tap were found using a network analyzer. It was found that once the plasma was ignited, all resonance properties of the design changed. The optimum tap position for maximum forward power then had to be found by trial and error, by noting the resonance frequency and the ratio of the input and reflected power. It was found that the quality of the connection between the tap and the coil, as well as the coaxial cable and the power wire also affected the resonance properties of the plasma source. For example, proper BNC connectors and a properly soldered connection between the wire tap and the coil increased the net forward power into the resonator.

The current design of the plasma source operates at 64% efficiency, with 110 watts of forward power into the resonator and 40 watts reflected at a frequency of 200 Mhz. A new design is being tested, which operates at 200 watts and 180 Mhz, with almost zero reflected power. An increase in forward power should increase the amount of reactive nitrogen produced, therefore increasing the amount of nitrogen in our samples.

2.4   X-Ray Diffraction Measurements

X-Ray diffraction (XRD) rocking curves are used to measure the amount of nitrogen in a sample. There are two peaks visible in the diffraction pattern shown in Figure 2.3. The one on the left is from the GaAs substrate and the weaker one on the right from the GaNAs top layer. As the amount of nitrogen in the sample increases, the lattice constant

decreases, and therefore the GaNAs peak shifts to the right, farther from the GaAs peak.
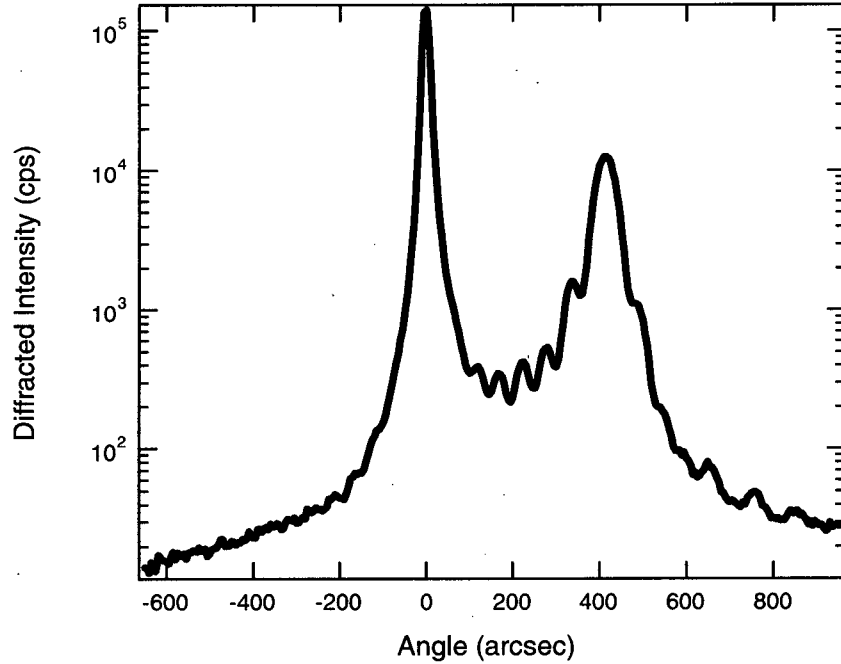
Figure 2.3: X-ray diffraction data of a sample containing 0.79% nitrogen.

One percent of nitrogen composition corresponds to 526 arcseconds splitting which follows from the lattice parameters and elastic constants of GaAs, and has been verified through secondary ion mass spectrometry (SIMS) experiments[15]. In Figure 2.3, we see that the distance between the two peaks is about 415 arcseconds and therefore we can conclude that there is 0.79 % nitrogen in that sample. The GaNAs layer thickness can also be accurately calculated by using the fringes on either side of the GaNAs diffraction peak.

2.5   Contact Deposition

The samples were first etched in an HCl solution for 5 minutes to remove the oxide buildup after exposure to air. Some samples were then annealed to 750°C for 60 seconds using a rapid thermal anealer. A GaAs wafer was placed over the sample so that the arsenic did not desorb from the surface during the anneal.

Contacts were deposited in a HV environment through a metal shadow mask using electron beam and thermal evaporation. For photoconductivity measurements, the mask was used to create five fingers on the sample surface as shown in Figure 2.4a. The fingers were 0.5 mm in width, spaced 1.0 mm apart. For Hall measurements, contacts were deposited on the corners of the sample using another mask as shown in Figure 2.4b. The sample holder was designed to allow contacts to be made on several samples at the same time. This not only saves time, but it ensures that the contacts and deposition conditions between annealed and as-grown samples are the same and therefore reduce inconsistencies between measurements.

For n-type samples, 150 nm of indium was thermally evaporated and then 10 nm of gold was deposited using electron beam evaporation. These contacts were annealed to 550°C for 30 seconds. For p-type samples, 12 nm of titanium, 10 nm of platinum and 100 nm of gold were deposited using electron beam evaporation and annealed to 500°C for 30 seconds. P-type contacts were used on undoped samples, as they show weak p-type characteristics. Current-voltage curves were measured to ensure the contacts were ohmic. Details of the growth conditions and different contact metals tested are described in Appendix A.
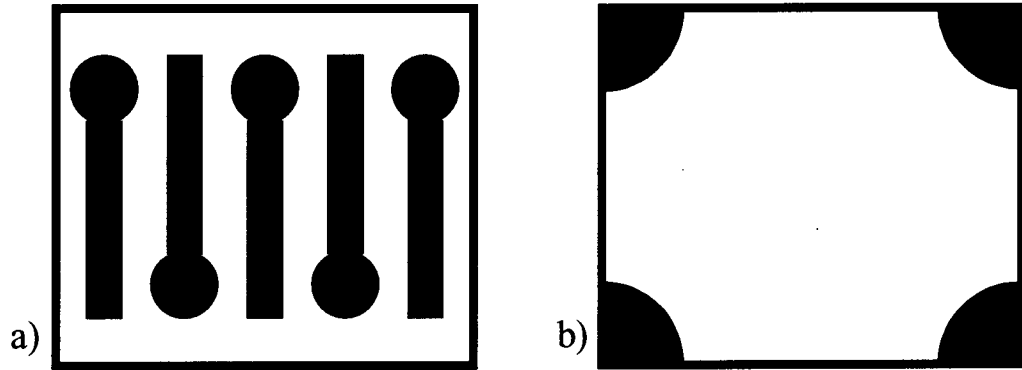
Figure 2.4: (a) The mask used for photoconductivity measurements creates five fingers on the sample surface. (b) The mask used for Hall measurements. This mask leaves small contacts on the corners of the samples.

2.6 Experimental Setup

The GaNAs samples grown show a relatively low resistivity and good photoresponse which is common for narrow bandgap semiconductors[16]. To extract the photocurrent from the dark current, a modulation technique is used. A tungsten light source is focused through a 680 nm filter to the monochromator, and the light output is chopped using a mechanical chopper set to 210 Hz. The filter prevents wavelengths below 680 nm from entering the monochromator, eliminating second order diffraction from the grating. The output is then focused onto a fibre bundle, which directs the monochromatic light onto the sample. Figure 2.5 shows the experimental setup used. The sample holder is made of stainless steel, and a piece of silicon is used to insulate the sample from the holder. Silicon is used because it is an electrical insulator but is thermally conductive. A cylindrical heater can be inserted into the sample holder to perform temperature dependent measurements, and a thermocouple can be attached to the sample holder.

To measure the photoconductivity, a constant current is applied to the two outer

680 nm
Filter   Lens

Monochromator   ◄⋯█⋯◖⋯⋯ W Lamp

Lens Chopper   Optical Fiber

Sample

IEEE Interface
Computer   Lock-in Amplifier   Sample Holder
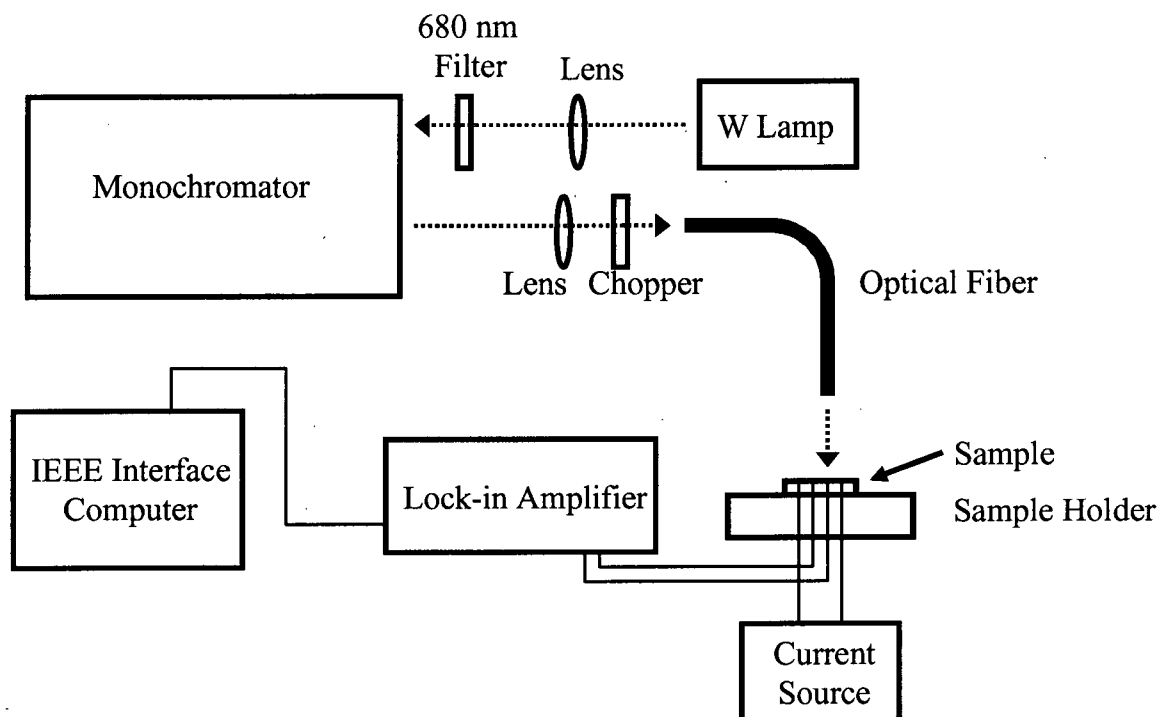
Current
Source

Figure 2.5: Experimental setup used to measure the photoconductivity of the samples.

contacts, and the voltage drop between two inner contacts is measured as a function of

wavelength, as shown in Figure 2.6. Typically a current between 1 μA and 1 mA is used.

The photoconductivity signal is measured using a lock-in amplifier to extract the AC voltage

signal between the two inner contacts. Alternatively the dark conductivity can be measured

using a voltmeter to measure the DC signal. Temperature dependent measurements can be

done by using a Variac to control the power to the heater and the temperature is recorded

by attaching a thermocouple to the sample holder.

All instrument readings are recorded with a computer through an IEEE interface.

The starting wavelength and the rate of increase are given to the acquisition program, and
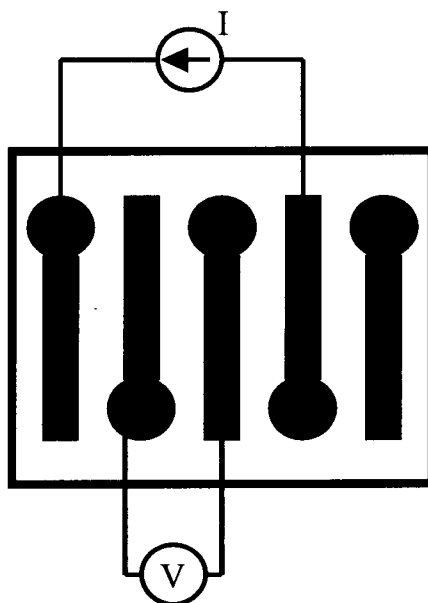
Figure 2.6: The contact configuration used to measure the optical properties. A constant current is applied to the two outer contacts and the voltage drop between the two middle contacts is measured. One contact is not used in the experiment.

the wavelength is then calculated for the entire experiment. Tests have verified that the monochromator runs at a constant rate, and finishes at the calculated wavelength over a 1000 nm range.

Chapter 3

Dark Conductivity

The electrical properties of semiconductors, such as the resistivity, charge carrier concentration and mobility are important to understanding their performance. To obtain these properties, a combination of a resistivity and Hall measurement is used. When a conductor with an applied current is placed in a magnetic field perpendicular to the direction of current, a voltage is generated perpendicular to both the current and the magnetic field[17]. This effect is known as the Hall effect and is the basis for the Hall measurements. For a square-shaped semiconductor with an applied current and magnetic field, the charge carriers travelling in the semiconductor experience a force, the Lorentz force, normal to their velocity and the direction of the magnetic field (see Figure 3.1). The Lorentz force deflects the charge carriers to one side of the semiconductor so that charge accumulates on the sides of the semiconductor. The voltage difference between the two sides of the semiconductor is known as the Hall voltage, V_H[17].

The Van der Pauw technique is commonly used for Hall measurements due to its

Lorentz Force F = -ev x **B**
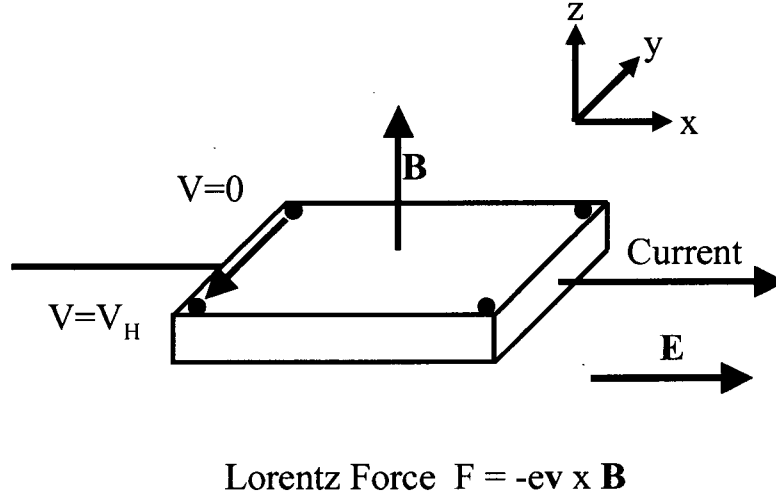
Figure 3.1: A sample used for Hall measurements. With an applied current in the x-direction and a magnetic field applied in the z-direction, the carriers feel a force in the y-direction which accumulates charge on the sides of the semiconductor.

simplicity[18][19]. Ohmic contacts are first deposited onto the corners of a square semiconductor, as described in section 2.5. There are a few conditions that must be observed when using the Van der Pauw technique: first, the semiconductor should not have any cracks or non-conducting islands. Second, the distance between contacts should be much greater than the area of the contacts. Third, it is important to know the relative directions of the magnetic field and applied current, as the sign of the Hall voltage tells you whether the majority charge carriers are the holes or electrons.

3.1 Hall Measurements

The resistivity of the sample is measured first in the absence of an external field. As shown in Figure 3.2, a current is applied between two contacts (1, 2) and the voltage drop

is measured between the other two contacts (3, 4).. The current is then reversed and the voltage drop is recorded. This measurement is repeated for a different contact configuration, and then the resistivity is calculated using

$$\rho_A = \frac{\pi}{4\ln 2}\frac{f_A t}{I}\left(V_{12,34} - V_{21,34} + V_{23,14} - V_{32,41}\right) \tag{3.1}$$

where t is the sample thickness, I is the applied current, $V_{12,34}$ is the voltage measured between contacts 3 and 4 when current is applied from contact 1 to contact 2, and f_A is the form factor which is described in appendix A. This method is then repeated except the contact points of the current and voltage tips are interchanged. The resistivity is then calculated using

$$\rho_B = \frac{\pi}{4\ln 2}\frac{f_B t}{I}\left(V_{34,12} - V_{43,12} + V_{41,23} - V_{14,23}\right) \tag{3.2}$$

where f_B is the form factor for this measurement. An average of the two resistivity measurements, ρ_A and ρ_B is taken to obtain ρ. The ratio of ρ_A and ρ_B is known as the Hall ratio and should be close to unity due to the symmetric nature of the measurement.

Now that the resistivity of the sample is known, the carrier concentration and mobility can be measured using the Hall effect. An electric field is created by applying a constant current between two contacts, and a magnet is used to create a field perpendicular to the applied current. The Hall factor R_H is measured using a similar probing method as described previously for the resistivity, and can be calculated using

$$R_{H_A} = \frac{10^8 t}{4IB}\left(V_{31,42}(+B) - V_{13,42}(+B) + V_{13,42}(-B) - V_{31,42}(-B)\right) \tag{3.3}$$
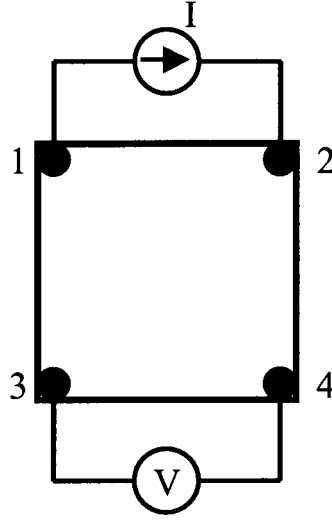
Figure 3.2: A diagram showing how $V_{12,34}$ is measured. A current is applied from contact 1 to contact 2, and the voltage drop between contacts 3 and 4 is recorded.

where B is the magnetic field measured in Gauss, $V_{31,42}(+B)$ indicates the measurement in a positive magnetic field and $V_{31,42}(-B)$ indicates the measurement in a negative magnetic field. The current and voltage contact tips are interchanged, and the Hall factor is then calculated using

$$R_{H_B} = \frac{10^8 t}{4IB} \left(V_{42,13}(+B) - V_{24,13}(+B) + V_{24,13}(-B) - V_{42,13}(-B) \right). \tag{3.4}$$

An average of R_{H_A} and R_{H_B} is taken to obtain the Hall factor R_H. The sign of R_H tells us whether the majority carrier is the electron or hole. If it is negative, then the majority carrier is the electron; if it is positive, the majority carrier is the hole. If the majority carrier is the electron, the electron mobility can be calculated using

$$\mu_n = \frac{-R_H}{\rho} \tag{3.5}$$

where ρ is the resistivity calculated previously. The electron concentration n can then be calculated using

$$n = \frac{1}{\rho e \mu_n}. \tag{3.6}$$

If the majority carrier is the hole, the hole mobility can be calculated using

$$\mu_p = \frac{R_H}{\rho} \tag{3.7}$$

and the hole concentration p can be calculated using

$$p = \frac{1}{\rho e \mu_p}. \tag{3.8}$$

3.2 Mobility

The mobility is related to the mean free path, which is determined by various scattering mechanisms. The two dominant sources of scattering mechanisms are lattice vibrations and impurities[16]. Impurity scattering results when a charge carrier moves past an ionized dopant impurity and the coulomb interaction between the impurity and the charge carrier deflects the path of the charge carrier. Alternatively, the charge carrier could scatter from a structural defect or a substitutional impurity. At room temperature, for low dopant concentrations (10^{14} cm^{-3}), lattice scattering dominates and at high ($>10^{17}$ cm^{-3}) concentrations, impurity scattering dominates[16].

In this thesis, the mobility of many p-type and n-type samples have been measured. It has been observed that the hole mobility is relatively unaffected by the addition of up
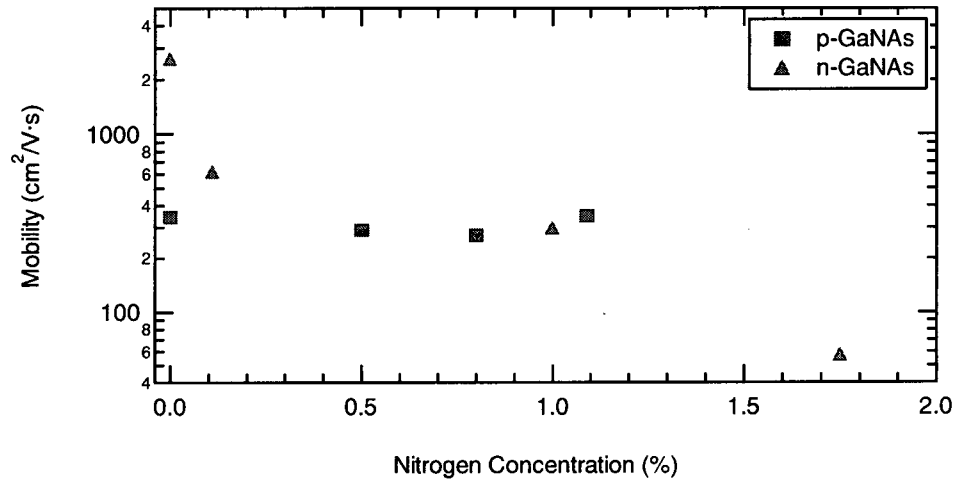
Figure 3.3: Mobility as a function of nitrogen concentration. Hole mobilities (indicated by the squares) are relatively unaffected while electron mobilities (indicated by the triangles) decrease with nitrogen content.

to 1% nitrogen content, as shown in Figure 3.3. The electron mobility is strongly affected by just a small amount of nitrogen, dropping from 3000 $cm^2/V \cdot s$ at 0% nitrogen to 250 $cm^2/V \cdot s$ at 1% nitrogen content.

There have not been any reported studies of the mobilities of GaNAs, however there are a few on InGaNAs which are of interest due to the similar nature of the two alloys. The doping levels were all approximately 10^{16} cm^{-3} for both n-type and p-type samples, and grown by MBE[15][20] or MOCVD[21]. Table 3.2 summarizes the electron and hole mobilities, the nitrogen concentration and the growth conditions used. These studies show that at high nitrogen concentrations the electron mobilities become very small[20], comparable to those of the hole mobilities[15][21]. These results agree with what we observed; for small amounts of nitrogen (up to 1%), the electron mobility drops dramatically. We did not observe a decrease in the hole mobility with nitrogen content up to 1%, however it is

InGaNAs Study	Growth Method	Nitrogen Concentration	Electron Mobility	Hole Mobility
Hong *et al.*[20]	MBE	1.5 %	-	130
Kurtz *et al.*[21]	MOCVD	2 %	60	100
Robinson *et al.*[15]	MBE	1.5 %	150	260

Table 3.1: Electron and hole mobilities of InGaNAs from various studies.

possible it would decrease at higher concentrations.

3.3 Carrier Concentration

When growing GaAs alloys, it is relatively easy to dope them with Be or Si and achieve a specified carrier concentration, however when nitrogen is added to p-type GaAs, we have observed a change in the expected carrier concentration. For low dopant concentrations (10^{14} cm^{-3}), an increase was observed with increasing nitrogen content and for high concentrations (10^{17} cm^{-3}) a decrease was observed with nitrogen content. We assume that the change in carrier concentration with nitrogen content is due to gap states associated with nitrogen, which affects the Fermi level. This is discussed in more detail in section 5.2.

Fleck *et al.*[22] observed in n-type and p-type InGaNAs alloys grown by MBE that the measured carrier concentration decreases for highly doped (10^{18}) samples with increasing nitrogen content. We observed similar effects.

3.4 Problems with Hall Measurements

The quality of the Hall measurements depends on the impurity doping concentrations. Undoped and low doped GaAs and GaNAs are highly resistive, and low currents

have to be used in the experiment which produce noisy signals and lead to large errors. For an ideal sample, when no magnetic field is applied, the magnitude of the voltage measured should be the same as when the current is reversed. Time may be required for the voltage to reach equilibrium. This happens very quickly for high-doped samples, and may take several minutes for undoped and highly resistive samples.

The resistance between two diagonally opposite corner contacts on a square sample should be roughly the same as the resistance between the other two corner contacts. In a square sample, the resistance between pairs of contacts along a cleaved edge, given equal separations should be roughly equal. This was not always observed. In a few cases, the resistances along three edges were roughly equal, but the resistance along the fourth edge was very different. It is unlikely this is due to cracks in the sample as none was observed under an optical microscope. Annealing to 750°C reduces or eliminates this problem, as discussed in the next section. These asymmetries are more prominent with lightly doped alloys which are more resistive, and have also been observed in other studies, where they comment that these asymmetries occur mostly at low carrier concentrations and low temperatures[21].

3.5 Annealing

Annealing to 750°C for 60 seconds before depositing contacts dramatically improves the quality of the Hall measurements performed as inferred from the Hall ratio. The annealed samples have Hall ratios closer to unity than as-grown samples. Annealing also reduces or eliminates the asymmetry issues discussed in section 3.4, where the resistance between two diagonal contacts is different than the resistance between the opposite diagonal

contacts.

We observed a small increase in the carrier concentration, and a marginal decrease of the mobility for p-type GaNAs after annealing as shown in Figures 3.4 and 3.5, respectively. Since the carrier concentration does not appreciably change, this is an indication the Fermi level does not move much and therefore the traps are not eliminated by annealing. This is in contrast with another study, which observed an increase in the p-type doping of GaNAs alloys after annealing[23]. In that study, the undoped GaNAs layer was sandwiched between two doped layers, so it is likely that the Be dopant diffused into the GaNAs layer creating a higher p-concentration. Be can diffuse at growth temperatures (600°C), but Si does not. In our experiments, the change in carrier concentration for n-type samples was very small with annealing; in some samples it increased and in others it decreased.

The small change in mobility and carrier concentration with annealing may be due to a combination of factors: first, the sample is not perfectly uniform and therefore pieces cleaved from different areas of the sample may be slightly different and second, there may be variations in the contacts. Although the contacts are deposited and annealed in nominally the same way, there may be small variations in how they are put down.
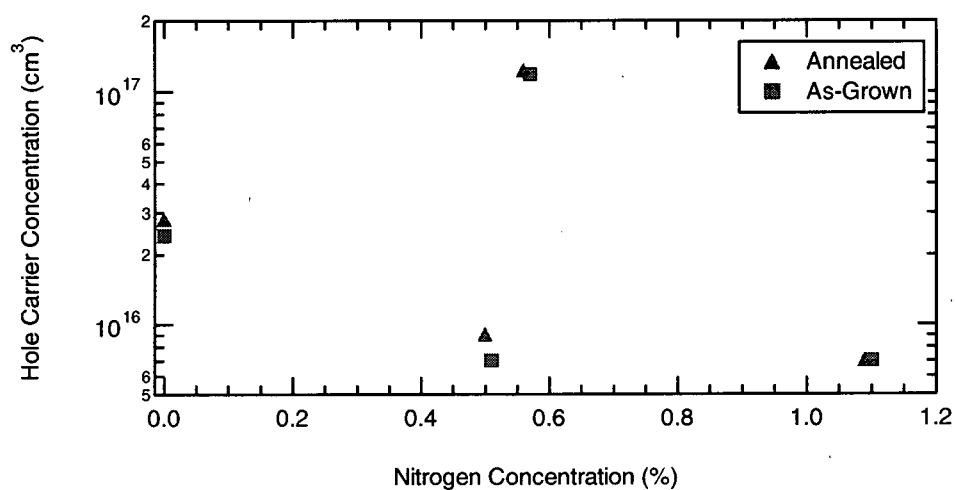
Figure 3.4: Change in hole concentration after annealing. A small increase was typically observed.
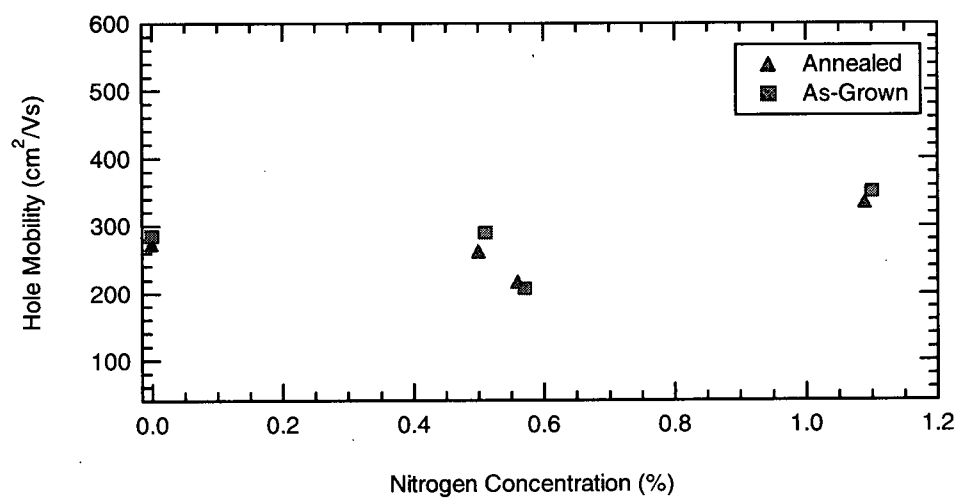
Figure 3.5: Change in hole mobility after annealing. A small decrease in the mobility was typically observed.

Chapter 4

Photoconductivity

4.1   Theory of Photoconductivity

Photoconductivity is the process whereby mobile charge carriers are created by absorption of incident radiation. In a semiconductor at room temperature in the dark, the conductivity is low because only a few electrons have sufficient energy to jump across the bandgap from the valence band to the conduction band. When an electron in the valence band absorbs a photon of sufficient energy it can be excited across the bandgap. Photoexcitation can occur through several optical absorption mechanisms depending on the wavelength of light, including band to band transitions, impurity level to band edge transitions, ionization of donors, and deep level to conduction band transitions[24]. Figure 4.1 illustrates these transitions.

Absorption of photons near the bandgap takes place when an electron is excited from the valence band to the conduction band. Two types of transitions are possible, direct and indirect transitions as shown in Figure 4.2. A direct transition occurs when the valence
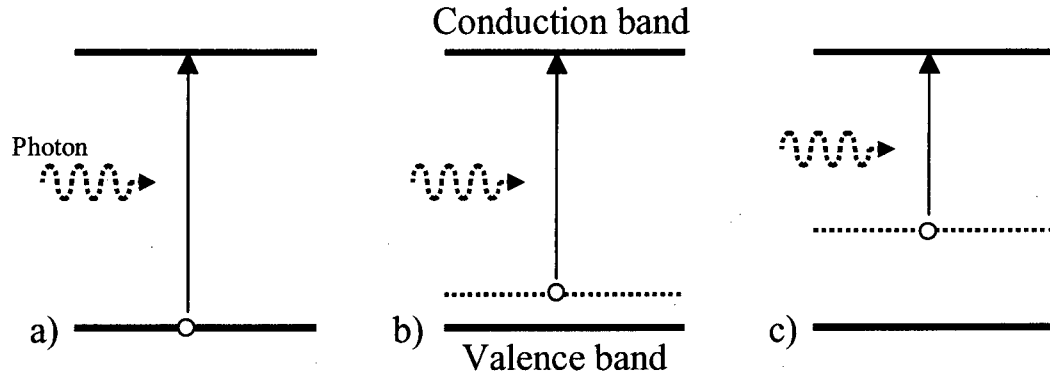
Figure 4.1: An example of three possible optical transitions which create free electrons: a) valence band to conduction band, b) impurity (acceptor) level to conduction band, and c) deep level to conduction band transition.

band maximum and conduction band minimum have the same crystal momentum and a photon excites an electron across the bandgap; indirect transitions occur when the crystal momenta at the valence band maximum and the conduction band minimum are different. In this case, phonon absorption or emission has to occur to conserve the crystal momentum of the system[25]. GaAs and GaNAs are both direct gap semiconductors[26] and indirect transitions will not be discussed further.

Generally there is a close correlation between the photoconductivity excitation spectrum and the optical absorption spectrum[24], although there are exceptional circumstances where a one-to-one correspondence is not observed. For example, if absorption takes place through transitions between two defect states in the bandgap there will be no contribution to the photoconductivity[24]. It is unlikely that this mechanism contributes much to the absorption coefficient in our case.

For incident radiation whose energy is below the bandgap of the semiconductor, there will not be sufficient energy to excite the electrons from the valence band to the
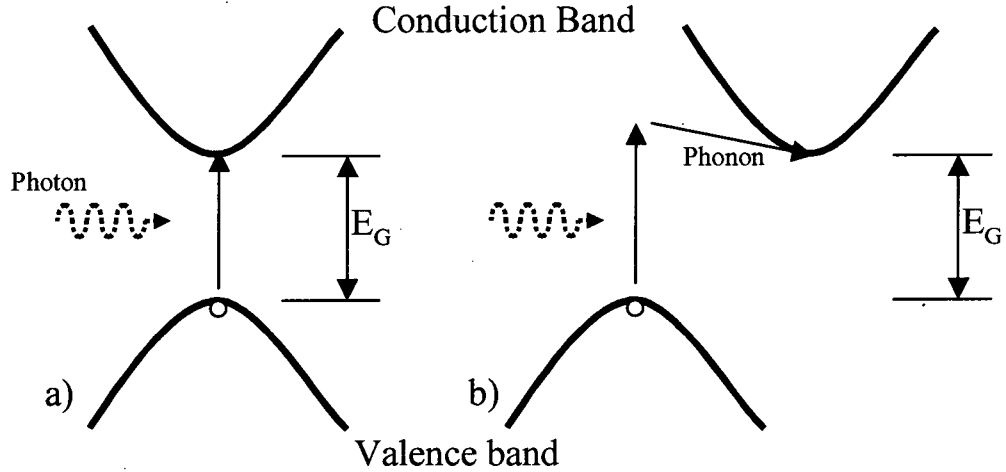
Figure 4.2: An example of direct and indirect transitions. In a direct transition, a photon of energy E_G is sufficient to excite the electron across the band gap (a). In an indirect transition, a phonon is also required (b).

conduction band. Once the incident radiation energy is equal to the bandgap energy, free carriers are produced and a large increase in the photoconductivity of the semiconductor is observed.

In direct transitions, the change in crystal momentum is zero in optical transitions. Therefore only photons with an energy equal to the bandgap or greater will be absorbed by a valence band electron. In other words interband transitions will take place if,

$$h\nu = E_C(0) - E_V(0) = E_G \tag{4.1}$$

or greater, where $h\nu$ is the energy of the photon, E_G is the energy of the bandgap, and E_C, E_V are the energies of the electrons in the bottom of the conduction band and top of the valence band, respectively.

The absorption coefficient is the inverse penetration depth measured in cm^{-1}. The

optical absorption spectrum for GaAs has several interesting features as shown in Figure 4.3. At low energies well below the bandgap, the absorption is dominated by free carriers[27]; at energies near the bandgap, an exponential increase in the absorption coefficient occurs which is due to the tails of the conduction and valence band densities of states[28]. In this region, we can write the absorption coefficient as an exponential,

$$\alpha(h\nu) = a_o \exp\left(\frac{h\nu - E_g}{E_o}\right) \tag{4.2}$$

where $\alpha(h\nu)$ is the absorption coefficient as a function of photon energy $h\nu$, and E_o is the characteristic energy of the Urbach edge, commonly referred to as the Urbach parameter[29]. As the energy increases, the absorption coefficient becomes less exponential and can be described by a parabolic band approximation. In the parabolic band approximation, the absorption coefficient is given by[24]

$$\alpha = \alpha_0 \left(h\nu - E_G\right)^{1/2} \tag{4.3}$$

where α_0 is a constant. This is a useful formula commonly used to obtain the bandgap energy of semiconductors from optical absorption data.

4.2 Photoconductivity Measurements

Experimental photocurrent spectra for three different samples containing 0%, 0.65% and 0.95% nitrogen are shown in Figure 4.4 as a function of wavelength. The spectra have all been normalized to unity at maximum values. The absorption edges are visible, with one at the GaAs bandgap around 875 nm, and the others at 975 nm and 1020 nm
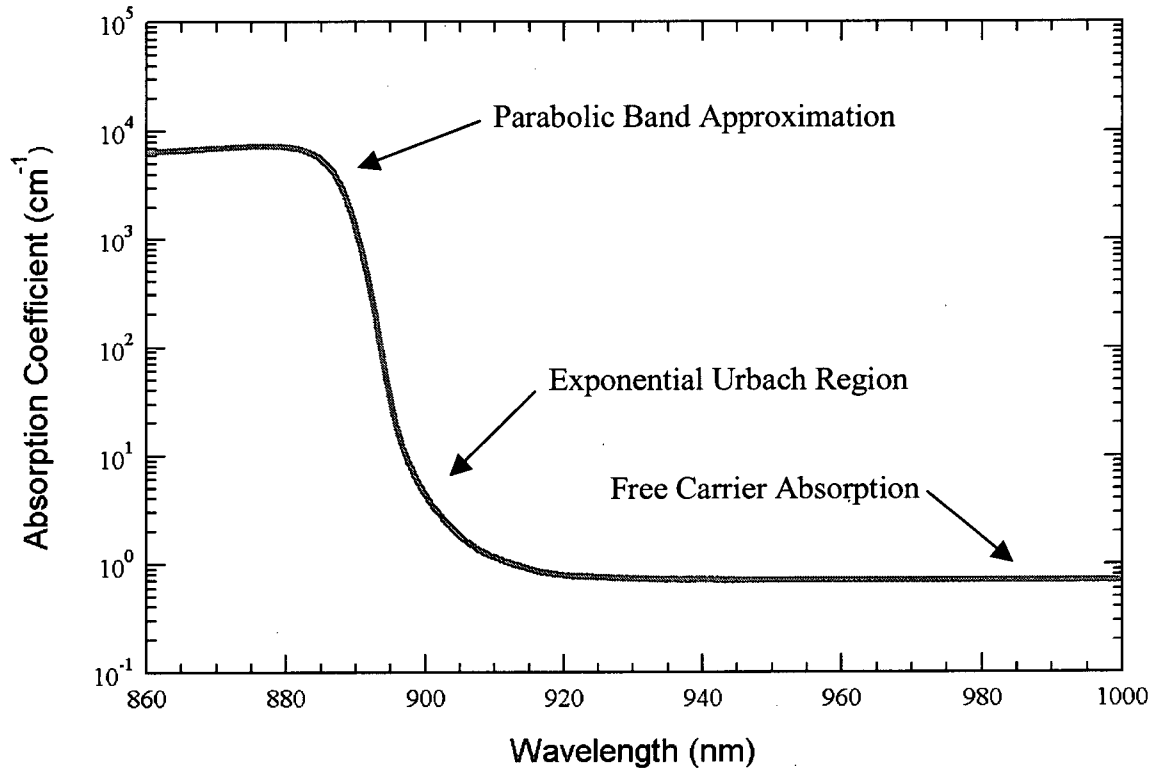
Figure 4.3: Schematic of the absorption coefficient for GaAs as a function of wavelength,

corresponding to the bandgaps of the two different GaNAs samples. As the nitrogen content

increases, the GaNAs absorption edge moves to larger wavelengths.

Another prominent feature is the exponential Urbach region on the long wavelength

side of the absorption edge. The absorption edge is quite sharp for GaAs, but the absorption

edge of GaNAs becomes less sharp as nitrogen is added. This will be discussed further in

section 4.2.2. The fact that the bandgap of GaNAs is lower than GaAs makes it possible to

measure the photoconductivity of the GaNAs layer, independently of the GaAs substrate.
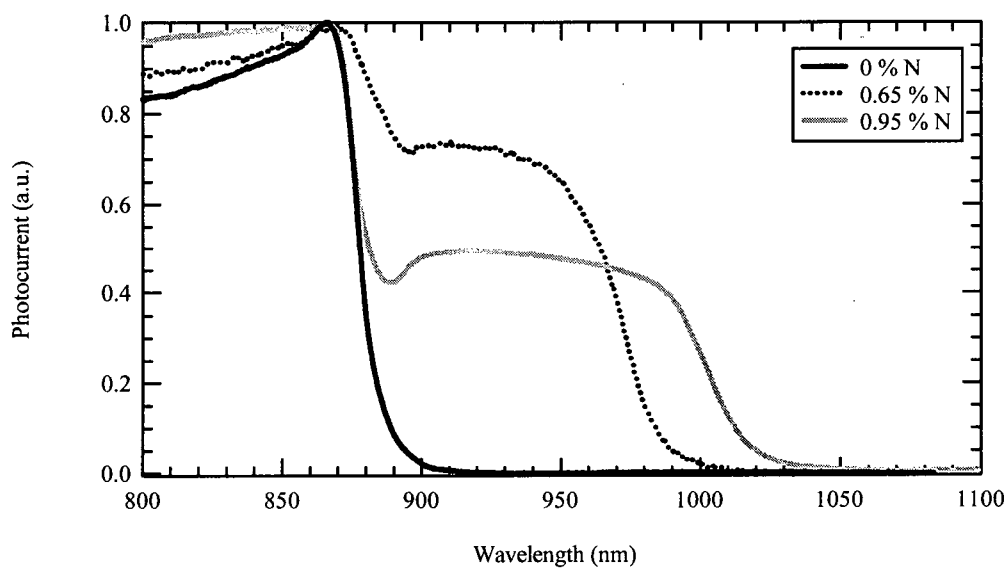
Figure 4.4: Experimental data for three different undoped samples containing 0%, 0.65% and 0.95% nitrogen.
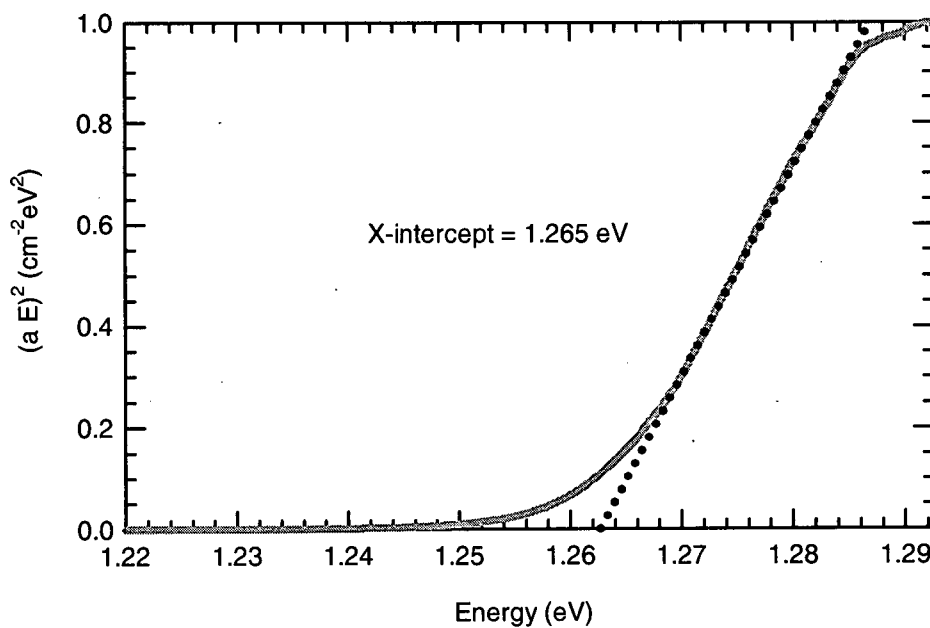
Figure 4.5: Photoconductivity as a function of energy normalized to incident flux, for a sample containing 0.79% nitrogen. The band gap is easily determined by extrapolating the linear part to zero.
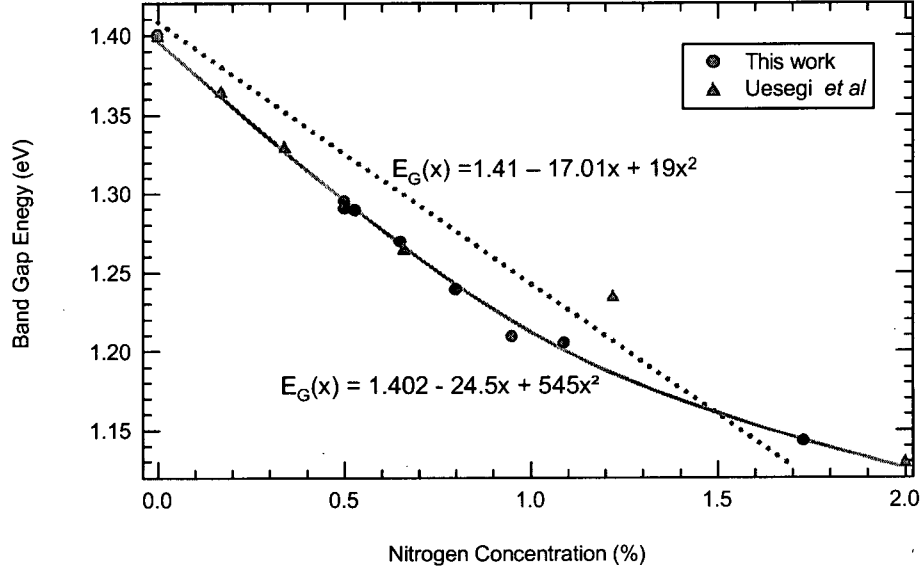
Figure 4.6: Band gap energy as a function of nitrogen content. The circles are data obtained using our photoconductivity measurements, and the triangles are data from Uesegi *et al.*[30] using optical absorption methods. The curve is a parabolic fit to the data given by equation 4.4, and the dotted line is a fit using equation 1.1.

4.2.1   Bandgap

The bandgap of the GaAs and GaNAs alloys can easily be determined from the photoconductivity spectrum. Using equation 4.3, the bandgap is the x-intercept on a graph of $(\alpha E)^2$ versus E as shown in Figure 4.5[3][30]. Our data agrees quite well with data by Uesegi *et al.*[30], as shown in Figure 4.6. The data also agrees with a parabolic fit,

$$E_G(x) = 1.402 - 24.5x + 545x^2 \qquad (4.4)$$

where x is the nitrogen mole fraction. The dashed line in Figure 4.6 is the bandgap calculated from equation 1.1 with a bowing parameter of -19 eV, as discussed previously. We observed that annealing does not change the measured bandgap. A blueshift has been ob-

served in the photoluminescence peak after anneal for GaNAs and InGaNAs quantum well (QW) structures[31], which indicates an increase in the bandgap, contrary to what we observed. The blueshift is attributed to out-diffusion of interstitial nitrogen from the growth. Since QWs are much thinner than the samples we have studied, it is likely that nitrogen out-diffusion is much stronger than in our thicker GaNAs samples.

4.2.2 Urbach Parameter

The optical absorption increases exponentially with increasing photon energy in the Urbach region. The exponential absorption edge is believed to be due to fluctuations in the electronic energy bands caused by lattice vibrations and structural or alloy disorder, which give rise to states below the band edge whose density decays exponentially towards midgap[28]. The inverse slope of the exponential absorption edge, E_o is commonly referred to the Urbach parameter[32]. Since the photoconductivity is proportional to the absorption coefficient, we use equation 4.2 to obtain the Urbach parameter by fitting a graph of $\ln(\alpha)$ versus $h\nu$; the inverse slope over the exponential region is the Urbach parameter, as shown in Figure 4.7.

GaAs buffer layers typically showed two distinct slopes in the Urbach region of the photoconductivity spectrum, as shown in Figure 4.8. This is likely due to the differences in the recombination lifetime of the GaAs substrate and the GaAs epi-layer. The photoconductivity measured is a combination of the photoconductivity of the GaAs substrate and the GaAs epi-layer,

$$\Delta\sigma \propto \tau_f F_f + \tau_s F_s \qquad (4.5)$$
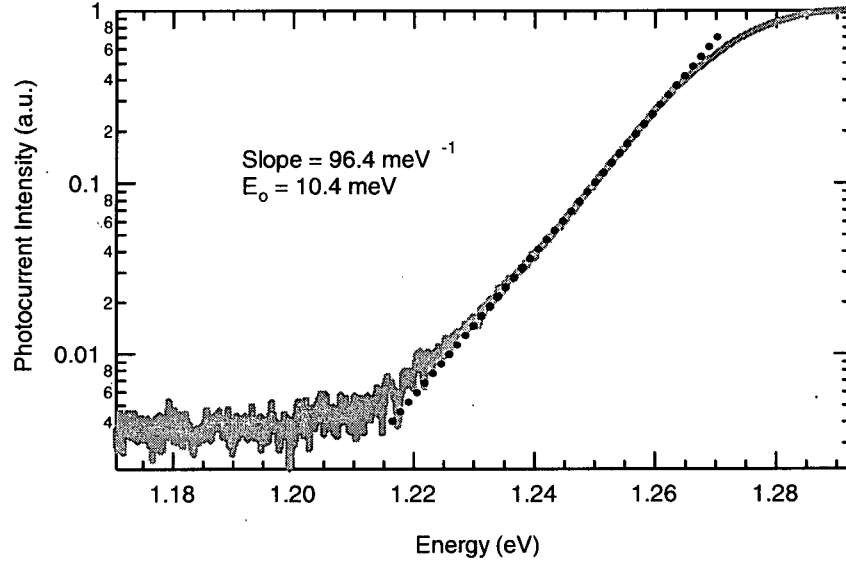
Figure 4.7: Photocurrent as a function photon energy normalized to the incident light flux for a sample containing 0.79% nitrogen. The Urbach parameter is obtained from a fit to the exponential region; the inverse slope is the Urbach parameter.

where F is the absorbed photon flux, τ is the recombination lifetime and the subscripts f and s refer to the film and substrate respectively. The flux of photons that are absorbed within a thickness t can be written as

$$F = \int_0^t \exp(-\alpha x)\mathrm{d}x \tag{4.6}$$

where α is the absorption coefficient defined in equation 4.2. We can therefore write equation 4.5 as

$$\Delta\sigma \propto \tau_f \int_0^t \exp(-\alpha x)\mathrm{d}x + \tau_s \int_t^L \exp(-\alpha x)\mathrm{d}x \tag{4.7}$$

where t is the film thickness and L is the substrate thickness. Solving the above equation yields

$$\Delta\sigma \propto \tau_f \left[1 - \exp(-\alpha t)\right] + \tau_s \left[\exp(-\alpha t) - \exp(-\alpha L)\right]. \tag{4.8}$$

A simulation of photoconductivity as a function of incident photon energy using equation 4.8 is shown in Figure 4.9, using a film thickness of 300 nm, substrate thickness of 350 μm, $E_o = 6$ meV and $E_g = 1.412$ eV for the expression in the absorption coefficient and a substrate recombination lifetime 60% of the epi-layer recombination lifetime.

At low energies, absorption is occurring mainly in the substrate. As the energy increases, the absorption in the substrate saturates and therefore the photoconductivity saturates at 1.39 eV, as shown in Figure 4.8. As the photon energy increases further, the film absorbs more of the photons. Eventually the absorption coefficient ceases to increase exponentially with photon energy when the energy is greater than the bandgap, and the photoconductivity saturates at 1.42 eV. The simulated photoconductivity spectrum in Figure 4.9 is in good qualitative agreement with the observed photoconductivity in Figure 4.8. It is expected that the fit could be further improved by taking into account surface and interface recombination.

Returning now to the Urbach parameter, we measured $E_o = 9.4$ meV for undoped GaAs, which is slightly higher than those of other studies, such as 7.5 meV[28], 6.7 meV[33] and 7.7 meV[34]. With the introduction of nitrogen, an increase in the Urbach parameter is observed for both p-type (Figure 4.10) and undoped (Figure 4.11) GaNAs. The Urbach parameters for the GaNAs alloys are higher than for GaAs, which is expected due to the increased disorder associated with the random N-alloying. The Urbach parameters are also higher for p-doped GaNAs than undoped GaNAs. The larger Urbach parameter in the
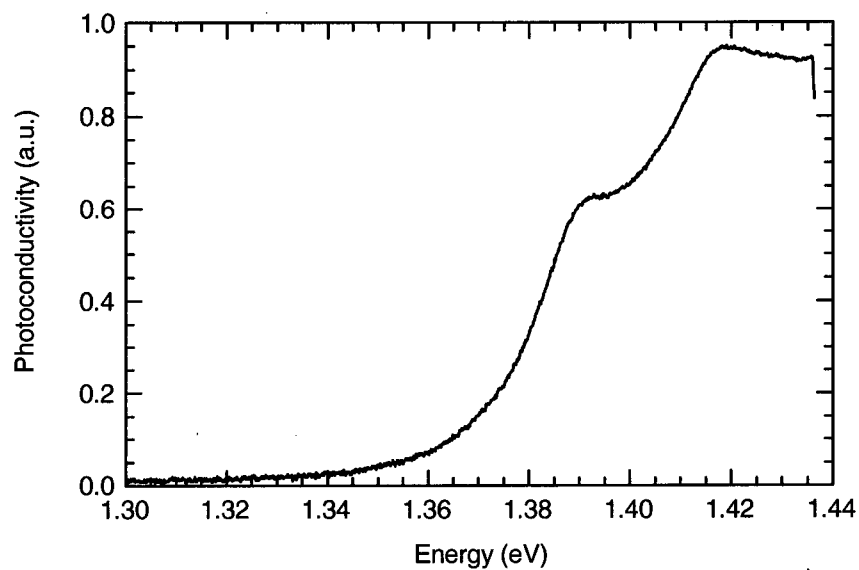
Figure 4.8: Photoconductivity measured for p-type GaAs as a function of wavelength, doped to 4.5×10^{14} cm^{-3}.
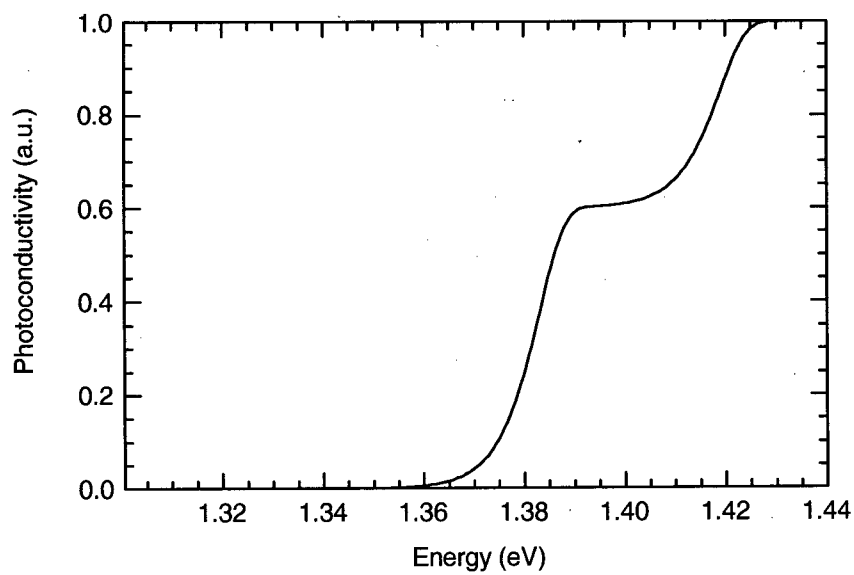
Figure 4.9: Photoconductivity simulation of a GaAs epi-layer on a GaAs substrate.

doped alloys is expected due to the random potentials associated with the donor impurities.

We attribute the increase in disorder with nitrogen content to composition fluctuations associated with the random distribution of nitrogen atoms in the crystal structure[4][21][35][36]. A scanning tunneling microscopy study found that the nitrogen atoms were distributed randomly with no evidence for long range fluctuations of the nitrogen atoms, in undoped samples grown by MOVPE[37]. The only deviation from a random distribution found was an increase in the number of nearest-neighbour pairs expected relative to a random distribution.

A comparison between as-grown and annealed InGaNAs samples showed no structural differences using scanning tunneling microscopy and scanning tunneling spectroscopy[38]. No differences in the atomic arrangements and the number of nitrogen-nitrogen pairs were detected.

Annealing reduced the measured Urbach parameter for all p-type samples, but not for all undoped samples, as shown in Figures 4.10 and 4.11. The Urbach parameter is a measure of the amount of disorder in the alloys, therefore we conclude that annealing has a positive effect on the disorder and the structural quality of the alloys. The sharpening of the Urbach edge will likely contribute a small blueshift to the room temperature photoluminescence.
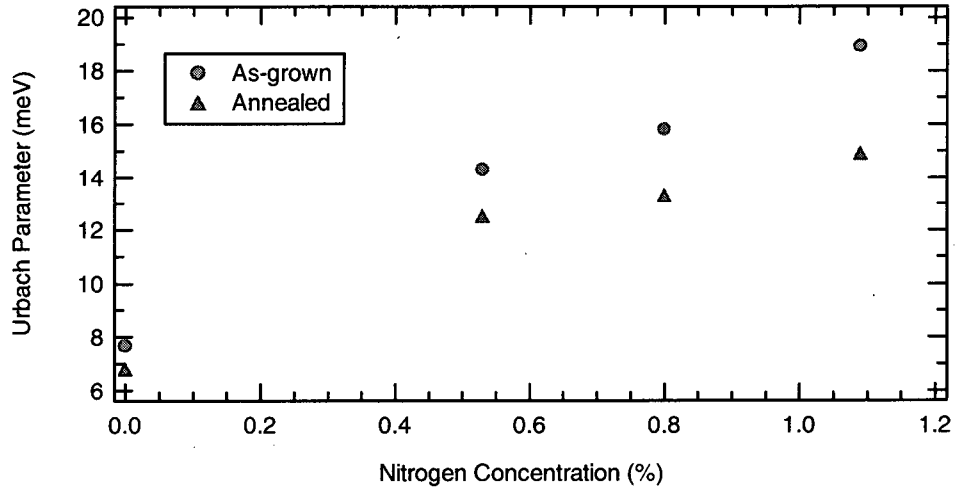
Figure 4.10: Urbach parameter for p-type ($p \simeq 10^{16}$ cm^{-3}) GaNAs as a function of nitrogen content. After annealing, the Urbach parameter decreased for all samples. The substrate temperature was ~460°C during growth.
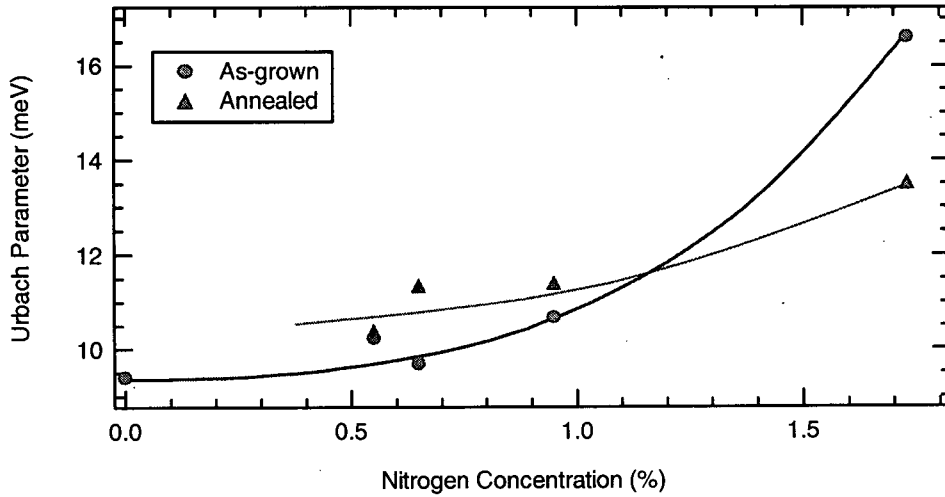
Figure 4.11: Urbach parameter for undoped GaNAs as a function of nitrogen content. Annealed samples are indicated by the triangles. The substrate temperature was ~490°C during growth. The curves are guides for the eye.

Chapter 5

Deep Levels in GaNAs

A shallow impurity level is created just below the conduction band by adding donors to a III-V semiconductor. There is usually enough thermal energy at room temperature to ionize all the electrons from the donor atoms to the conduction band, leaving a level of positive donor ions below the conduction band and mobile electrons in the conduction band. Under complete ionization, we can write the electron concentration as

$$n = N_D \qquad (5.1)$$

where N_D is the donor concentration. In the non-degenerate limit the Fermi level E_F (E_F more than a few KT from the band edge) is given by

$$E_C - E_F = kT \ln \left[\frac{N_C}{n} \right] \qquad (5.2)$$

where k is the Boltzmann constant, T is the temperature in Kelvin, E_C is the conduction band energy and N_C is the effective density of states in the conduction band. We see

from equation 5.2 that as the donor concentration increases, the energy difference $E_C - E_F$ decreases, or in other words the Fermi level moves closer to the conduction band. Similarly, adding an acceptor such as Be to a semiconductor creates an energy level just above the valence band. At room temperature, these impurity atoms accept an electron from the valence band, leaving holes behind. For complete ionization, the hole concentration is

$$p = N_A \tag{5.3}$$

where N_A is the acceptor concentration. As before in the non-degenerate limit, the Fermi level is given by

$$E_F - E_V = kT \ln\left[\frac{N_V}{p}\right] \tag{5.4}$$

where N_V is the effective density of states in the conduction band. As the hole concentration increases, the energy difference $E_F - E_V$ decreases, or in other words the Fermi level moves closer to the valence band.

If both donor and acceptor impurities are present, the conductivity type is determined by the impurity that is in greater concentration[16]. The Fermi level must shift to preserve charge neutrality, so that the total negative charges (electrons and ionized acceptors) and the total positive charges (holes and ionized donors) must be equal. For n-type semiconductors, the electron is the majority charge carrier while the hole is the minority charge carrier; for p-type semiconductors, the hole is the majority charge carrier while the hole is the minority charge carrier.

Study	Nitrogen Concentration	Energy Levels in GaNAs	Energy Levels in InGaNAs
Tanaka *et al.*[23]	0.3 %	0.21, 0.33, 0.58 eV	-
Krispin *et al.*[39]	3 %	0.16 - 0.18, 0.39 eV	-
Abulfotuh *et al.*[40]	2-3 %	0.13 0.17 - 0.22 eV	0.18-0.21 eV
Kwon *et al.*[41]	2.2 %	-	0.10, 0.23 eV

Table 5.1: A summary of traps in GaNAs and InGaNAs from various studies.

5.1 Trap Identification in GaNAs

Deep levels in GaNAs and InGaNAs alloys grown by MBE[39], MOVPE[23][40], and MOCVD[41] have been studied using deep level transient spectroscopy (DLTS). Several hole and electron traps have been identified in these alloys. We will concentrate on shallow traps that are unique to GaNAs and InGaNAs compared to GaAs and InGaAs. Table 5.1 summarizes the energy levels of the nitrogen related traps found.

A trap at 0.2 eV above the valence band is observed in several studies in both InGaNAs and GaNAs, but not in GaAs or InGaAs. This shallow trap is likely due to a nitrogen related defect[23][40]. We also observed a trap at 0.2 eV which will be discussed further in the next section.

Abulfotuh *et al.*[40] found two traps in dilute (2%-3%) p-type GaNAs alloys grown by MOVPE. They identified a trap at 0.13 eV, but it only occurred in some of the samples. There is no explanation given for this trap. They identified another trap at 0.17-0.22 eV with a concentration around 1.4×10^{15} cm^{-3}. The concentration and energy level is dependent on the amount of nitrogen in the alloy; as the nitrogen content increased, the trap energy level decreased. A possible explanation given is that this trap is affected by carbon impurities which are present in MOVPE samples, which then form complex C-N

states. They also observed a hole trap between 0.18 and 0.21 eV in the InGaNAs sample with similar characteristics to the one observed in the GaNAs sample. Several GaAs and InGaAs samples were grown, and none exhibited the above-mentioned traps. Therefore it was concluded that this shallow trap is associated with nitrogen. It was not mentioned if the samples had been annealed.

Tanaka et al.[23] observed three traps in their GaNAs samples grown by MOVPE. The undoped GaNAs layer, with 0.3 % nitrogen was sandwiched between n-type and p-type GaAs layers. Using DLTS, they observed traps at 0.21, 0.33 and 0.58 eV above the valence band, of which the dominant trap was at 0.58 eV. Although the concentrations of two traps decreased after annealing, the trap at 0.33 eV increased. They attributed this result to the fact that their anneal process was not optimized, and it is possible that arsenic vacancy type defects were created. They speculate the trap at 0.21 eV is a nitrogen related one, but are unsure whether it is intrinsic to the material system or produced during growth.

Krispin et al.[39] obtain slightly different results, where they find that the dominant traps are located at 0.35 and 0.45 eV above the valence edge for an undoped GaAs/ GaNAs/ GaAs heterojunction. Their samples were grown by MBE with 3% nitrogen. They identify a trap at 0.17 eV, consistent with other studies but they say that this level is also identified by release spectroscopy, and since peaks in release spectroscopy originate solely from spatially confined electronic states, this trap is located at the GaAs/GaNAs interface[42]. They also note that the density of the trap decreases inside the GaNAs layer, which is sandwiched between two GaAs layers, and therefore this trap does not originate from the GaNAs layer itself. This trap is relatively unaffected by annealing, but the concentration of the other

traps are reduced. The origin of the trap is not clear; they suggest that it is due to an intrinsic lattice imperfection, which is generated at the GaAs surface when the growth conditions are slightly modified by the RF Plasma. This is unlikely, as other methods of growth with no plasma source (MOVCD, MOVPE) show a trap at a similar energy level.

Other traps they find in the sample at 0.39 eV are identical to known hole traps in GaAs. They originate from an antisite defect, namely a gallium atom sitting on an arsenic site[43]. The traps at 0.35 eV and 0.55 eV are identical to those of Fe and Cu atoms on gallium sites commonly found in GaAs. They point out that these impurities are likely from operating the plasma source.

Kwon et al.[41] identify a number of traps at 0.10, 0.23 and 0.48 eV above the valence band in p-type InGaNAs containing 2% nitrogen, grown by MOCVD. The trap densities were all 10^{14} cm^{-3}, and a decrease in the trap concentration was observed after annealing, except at the 0.48 eV level. They speculate that the origin of the traps at 0.10 and 0.23 eV is likely due to a distribution of isolated point defects and/or point defect clusters, since upon anneal the concentrations are reduced.

5.2 Experimental Evidence for a Trap in GaNAs

GaAs samples can be grown with a specific doping level with good accuracy using MBE, and are very reproducible[44]. We have noticed that the addition of dilute amounts of nitrogen dramatically affects the doping levels in our samples. For GaAs grown with a p-doping level of 2.5 x 10^{16} cm^{-3}, we see a decrease in the measured carrier concentration with the addition of nitrogen; for GaAs grown with a p-doping level of 4.5 x 10^{14} cm^{-3} we

see an increase in the carrier concentration with the addition of nitrogen. Using equation 5.4, the Fermi levels for hole concentrations of 4.5 x 10^{14} cm^{-3} and 2.5 x 10^{16} cm^{-3} are 0.251 eV and 0.147 eV above the valence band edge, respectively.

The change in carrier concentration with nitrogen suggests that a trap level is created somewhere between the two Fermi levels. The density of these traps increases with nitrogen concentration. If we plot the hole concentration as a function nitrogen content, as shown in Figure 5.1, we see that the carrier concentration converges to a specific level. We speculate that this convergence corresponds to the hole concentration when the Fermi level is pinned at the level of the trap, with a concentration of 7 x 10^{15} cm^{-3}. We can estimate the energy level of the trap by using equation 5.4, where N_v is the effective density of states of the valence band,

$$N_V = \left(\frac{2\pi m_p kT}{h^2}\right)^{3/2} \tag{5.5}$$

where m_p is the hole effective mass and h is Planck's constant. The hole effective mass has not been experimentally measured for GaNAs as of this writing, however we will assume that the hole effective mass for GaNAs is similar to GaAs, as the valence band is believed to shift very little with the addtion of nitrogen[9]. The hole effective mass of GaAs is $0.42m_0$[16], where m_0 is the electron rest mass of 9.11×10^{-31} kg. Assuming the Fermi level is pinned by the trap and using equation 5.4, we can calculate that the energy level for the trap in the GaNAs alloy is 0.18 eV above the valence band, similar to the energy level observed in other studies discussed previously.

We can model the behaviour shown in Figure 5.1 using conservation of charge in
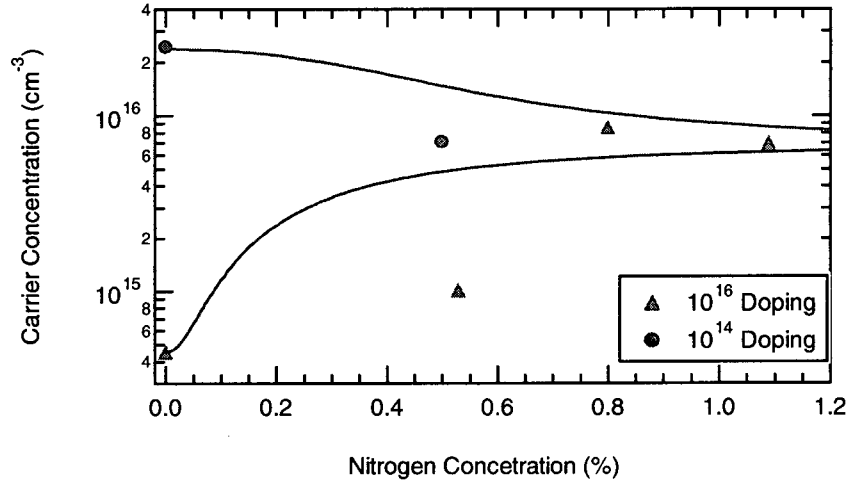
Figure 5.1: Carrier concentration as a function of nitrogen content. The circles are samples doped to $2.5\text{x}10^{16}$ cm^{-3} and the triangles are samples doped to $4.5\text{x}10^{14}$ cm^{-3}. The solid lines represent simulations using equation 5.15.

the bandgap. Free holes in the valence band have a charge concentration of

$$p = N_V(1 - f_V) \tag{5.6}$$

where N_V is the concentration and f_V is the Fermi-Dirac distribution function at an energy E_x, given by

$$f_x = f(E_x) = \frac{1}{1 + \exp(\frac{E_x - E_F}{kT})} \tag{5.7}$$

where k is the Boltzmann constant, T is the temperature and E_F is the Fermi energy level. Doping the alloy with Be creates an acceptor impurity level $E_A = 0.028$ eV above the valence band[16], which has a negative charge concentration of

$$N_A^- = N_A f_A \tag{5.8}$$

where N_A is the acceptor density. From the earlier discussion, we calculated a trap level at 0.18 eV above the valence band using equation 5.4. The net charge on the trap level is

$$N_t^- = N_t(2f_t - 1). \tag{5.9}$$

If the trap level contains two electrons, it is occupied ($f_t = 1$) and therefore negative, and if the trap level contains zero electrons, it is unoccupied ($f_t = 0$) and therefore positive. Using conservation of charge and substituting equations 5.6, 5.8 and 5.9, we have

$$N_A f_A + N_t(2f_t - 1) = N_V(1 - f_V). \tag{5.10}$$

Substituting the Fermi-Dirac distribution function into the above equation we have

$$N_A \frac{1}{1 + \exp(\frac{E_A - E_F}{kT})} + N_t\left(\frac{2}{1 + \exp(\frac{E_t - E_F}{kT})} - 1\right) = N_V\left(1 - \frac{1}{1 + \exp(\frac{E_V - E_F}{kT})}\right). \tag{5.11}$$

We can simplify this equation by noting that $(E_A - E_F)/kT$ is large and negative, so that

$$\frac{1}{1 + \exp(\frac{E_A - E_F}{kT})} \simeq 1, \tag{5.12}$$

and we can set $E_V = 0$ by using the valence band as our reference energy level so that

$$1 - \frac{1}{1 + \exp(\frac{E_V - E_F}{kT})} \simeq \exp\left(\frac{-E_F}{kT}\right), \tag{5.13}$$

for $E_F/kT \gg 0$, and noting that

$$\frac{2}{1 + \exp(\frac{E_t - E_F}{kT})} - 1 = -\tanh\left(\frac{E_t - E_F}{2kT}\right), \tag{5.14}$$

so that we finally have

$$N_A = N_V \exp(-\frac{E_F}{kT}) + N_t \tanh\left(\frac{E_t - E_F}{2kT}\right).$$ (5.15)

We can use this equation to simulate the Fermi level position for both low doped $(10^{14}$ cm$^{-3})$ and high doped $(10^{17}$ cm$^{-3})$ GaNAs alloys as a function of nitrogen content. Since GaAs is not known to contain a trap at 0.18 eV, we can calculate N_A for both doping levels by setting $N_t = 0$ at 0% nitrogen content. If the density of traps, N_t increases quadratically with nitrogen content (expected if the defects were associated with N-N clusters), we can write

$$N_t = \left(\frac{[N]}{0.005}\right)^2 N_{t,0.5}$$ (5.16)

where $N_{t,0.5}$ is the trap density at 0.5% nitrogen and $[N]$ is the nitrogen concentration. The trap level E_t was estimated by running simulations to find the best fit curves for the experimental data using equations 5.15 and 5.16. The results are shown in Figure 5.1. It was assumed that the trap level did not change with nitrogen concentration. The best fit simulations had a trap level of 0.18 eV, and a trap density of 2.5x10^{16} cm^{-3} at 0.5 % nitrogen content, and 10^{17} cm^{-3} at 1.0 % nitrogen content.

Other studies have measured a trap level at around 0.18 eV, such as Abulfotuh et al.[40] who measured a nitrogen level between 0.17 and 0.22 eV, Tanaka et al.[23], who measured 0.21 eV after annealing with 0.3% nitrogen and Krispin et al.[39], who measured 0.20 eV. These comparisons are summarized in table 5.2. The nitrogen related level we observed, not seen in GaAs, is clearly in agreement with other studies.
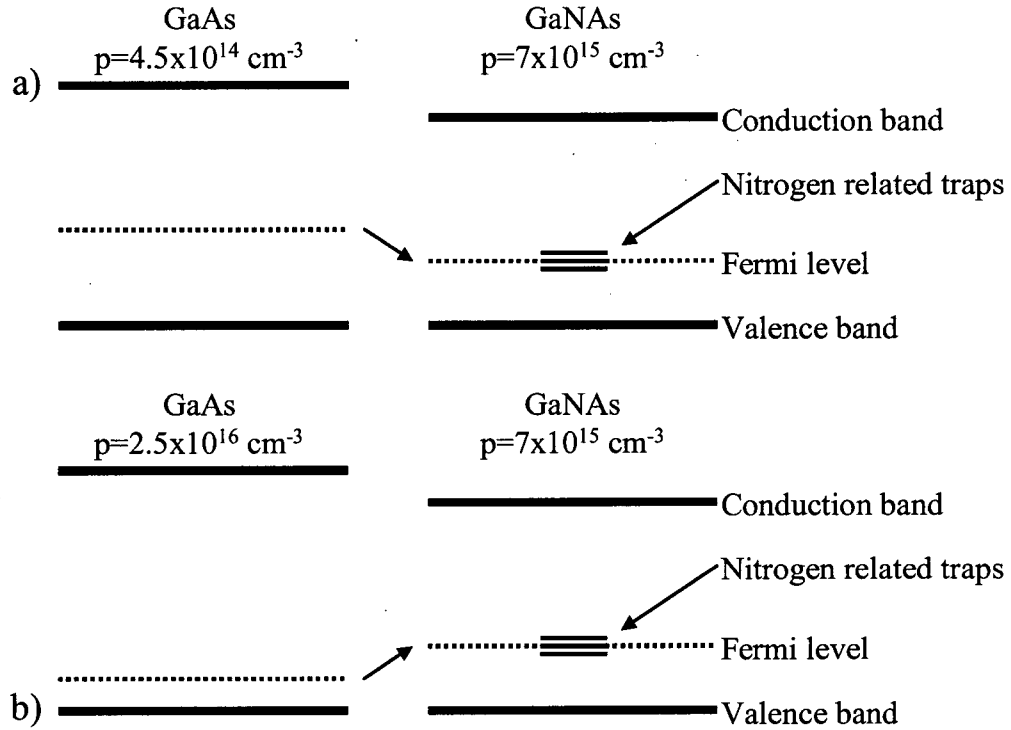
Figure 5.2: Schematic showing the change in Fermi level with the addition of nitrogen to GaAs. The Fermi level shifts and becomes pinned in the nitrogen related traps.

Figure 5.2 shows the behaviour of the Fermi level as nitrogen is incorporated into the GaAs alloy. The traps at 0.18 eV above the valence band shift the Fermi level closer to the trap level. At higher nitrogen concentrations ($>$0.8 %) the Fermi level becomes pinned at the trap level so that the measured carrier concentration is independent of the initial doping concentration. We did not notice a change in the carrier concentration after annealing, and therefore conclude that the Fermi level did not shift after annealing. This is evidence that the trap is not removed by annealing. This is in agreement with other studies, shown in table 5.2, which also show that the trap is resistant to annealing. Note that Tanaka *et al.*[23] observed a change in the carrier concentration after annealing, however they used

Author	Energy Level in GaNAs	Nitrogen Concentration	Anneal Effects
This Study	0.18 eV	0 - 1.1 %	No effect
Krispin et al.[39]	0.20 eV	3 %	No effect
Tanaka et al.[23]	0.21 eV	0.3 %	Increase in carrier concentration
Abulfotuh et al.[40]	0.17 - 0.22 eV	2 - 3 %	N/A

Table 5.2: Summary of energy levels due to nitrogen and the effect of annealing.

a very thin sample sandwiched by doped layers and it is likely Be diffused into the GaNAs layer, as discussed in section 3.5.

5.3 Density of Recombination Centers

The recombination lifetime and the density of recombination centers can be estimated from the magnitude of the photoconductivity signal. The hole lifetime is given by

$$\tau = \frac{\Delta\sigma}{F\alpha e\mu} \tag{5.17}$$

where F is the flux of incident radiation, α is the absorption coefficient, e is the electronic charge, μ is the hole mobility and $\Delta\sigma$ is the photoconductivity[16]. From this expression, the density of recombination centers can then be calculated using

$$N_R = \frac{1}{v_{th}s\tau} \tag{5.18}$$

where v_{th} is the thermal velocity (10^7 cm/s) of the charge carriers and s is the recombination cross section (10^{-15} cm^2). The photosignal in the experiment, ΔV, is measured

using a lock-in amplifier whose output is in volts. The photovoltage can be converted into photoconductivity, using

$$\Delta\sigma = \frac{\Delta V \sigma}{RI} \tag{5.19}$$

where σ is the dark conductivity, I is the bias current and R is the (dark) resistance of the sample. Figure 5.3 shows the density of recombination centers for p-type GaNAs as a function of nitrogen concentration using equation 5.18. Overall there was an increase in the density of recombination centers with the addition of nitrogen, which can be described with a parabolic fit

$$N_r = a + 10^{20} x^2 \tag{5.20}$$

where x is the nitrogen concentration, and $a = 2 \times 10^{15}$ cm^{-3} and 2×10^{16} cm^{-3} for as-grown and annealed samples, respectively. An increase in the density of recombination centers as a function of x^2 would be expected if the defects were associated with N-N dimers.

The dotted line in Figure 5.3 corresponds to the trap density calculated using a modification of equations 5.16 and 5.20,

$$N_r = a + \left(\frac{[N]}{0.005}\right)^2 N_{t,0.5} \tag{5.21}$$

where $a = 6 \times 10^{15}$ cm^{-3} and $N_{t,0.5}$ is the density of trap levels at 0.5% nitrogen, calculated previously in section 5.2. The density of recombination centers measured using the photoconductive lifetime are in good agreement with the density of trap levels simulated in 5.2 using conservation of charge.
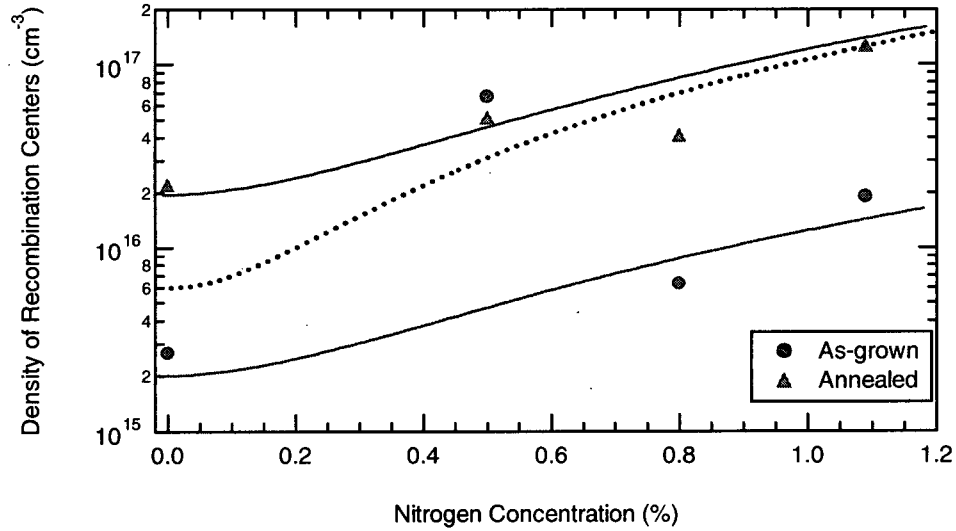
Figure 5.3: Density of recombination centers as a function of nitrogen content for p-type ($p \simeq 10^{16}$ cm^{-3}) GaNAs. The density of recombination centers increases with both annealing and nitrogen concentration. The dotted line corresponds to a trap density calculated using equation 5.21. The substrate temperature was ~460°C during growth.

Upon annealing, we have observed an increase in the density of hole recombination centers. This is opposite to the effect that is observed after annealing on the photoluminescence efficiency, which shows a reduction in the density of recombination centers[1][45]. Since the photoluminescence is dominated by the minority carrier lifetime and photoconductivity is dominated by the majority carrier lifetime, it is theoretically possible to increase the photoluminescence efficiency while decreasing the photoconductive recombination lifetime. In this case, we would see different annealing behaviour in the photoconductivity of p-type or n-type samples. It is not known why the as-grown point at 0.5% nitrogen is an order of magnitude higher than the other points in Figure 5.3.

Chapter 6

Conclusion

In this thesis, we have described a method for measuring the electronic and optical properties of dilute nitrides using photoconductivity. The GaNAs bandgap was found to decrease with increasing amounts of nitrogen. The bandgap decreased from 1.412 eV with 0% nitrogen to 1.29 eV with 0.5% nitrogen, and to 1.14 with 1.7% nitrogen. A change in bandgap was not observed upon annealing.

The Urbach parameter is a measure of the amount of structural and thermal disorder in the alloy. We observed an increase in the Urbach parameter for both undoped and p-doped GaNAs with increasing nitrogen content. The Urbach parameter for undoped GaAs increased from 9.4 meV to 12 meV with 0.5% nitrogen content, and p-doped GaAs increased from 8 meV to 14 meV with 0.5% nitrogen content. Annealing generally decreased the Urbach parameter, indicating a decrease in the disorder of the alloy.

The electron mobility of GaNAs alloys doped to 10^{17} cm^{-3} was found to decrease sharply with nitrogen content, from 3000 cm^2/V·s for 0% nitrogen, to 650 cm^2/V·s with

just 0.1% nitrogen, and to 250 cm^2/V·s with 0.5% nitrogen content. This behaviour is in agreement with that of other studies that reported a large decrease in the electron mobility with nitrogen content. The hole mobility was not affected with the addition of nitrogen up to 1%. High electron mobilities are very important for certain semiconductor devices, such as heterojunction bipolar transistors (HBTs).

The density of recombination centers can be calculated by measuring the magnitude of the photoconductivity signal. The density of recombination centers increased from 3x10^{15} cm^{-3} for 0% nitrogen content, to 2x10^{16} cm^{-3} for 1.1% nitrogen content. Upon annealing, an increase in the density of recombination centers was observed.

By examining the doping efficiency of p-type GaNAs as a function of nitrogen concentration, we conclude there is a trap at 0.18 eV above the valence band with a density of 2.5x10^{16} cm^{-3} at 0.5% nitrogen content and 10^{17} cm^{-3} at 1.0% nitrogen content. The trap level is in excellent agreement with other studies, such as Abulfotuh *et al.* who measured between 0.17 and 0.22 eV, Tanaka *et al.*, who measured 0.21 eV and Krispin *et al.*, who measured 0.20 eV. This trap may be the recombination center observed in photoconductivity measurements.

We present evidence that the density of defects in nitride alloys increases faster than linearly with nitrogen concentration, as one would expect for defects associated with N-clusters.

In summary, we have shown that photoconductivity measurements are a valuable tool in determining the quality of semiconductors. We have shown that the bandgap decreases with increasing nitrogen content and the Urbach parameter increases with nitrogen

content, which indicates an increase in the disorder of the alloy. Using Hall measurements, we have observed a decrease in the electron mobility with increasing nitrogen content, and the hole mobility was unaffected by up to 1% nitrogen. We have observed a trap level at 0.18 eV above the valence band edge by modelling the change in carrier concentration as a function of nitrogen, and obtained estimates for its density from the doping efficiency and photoconductive recombination lifetime.

Bibliography

[1] I.A. Buyanova, W.M. Chen, and B. Monemar. *MRS Internet J. Nitride Semicond. Res.*, 6:2, 2001.

[2] I. Suemune, K. Uesugi, and W. Walukiewicz. *Appl. Phys. Lett.*, 77:3021, 2000.

[3] G. Pozina, I. Ivanov, B. Monemar, J.V. Thordson, and T.G. Andersson. *J. Appl. Phys.*, 84:3830, 1998.

[4] Y. Qiu, S.A. Nikishin, H. Temkin, N.N. Faleev, and Y.A. Kudriavtsev. *Appl. Phys. Lett.*, 70:3242, 1997.

[5] X. Liu, M.E. Pistol, L. Samuelson, S. Schwetlick, and W. Seifert. *Appl. Phys. Lett*, 56:1451, 1990.

[6] A. Lindsay and E.P. O'Reilly. *Solid State Communications*, 112:443, 199.

[7] S.H. Wei and A. Zunger. *Phys. Rev. Lett.*, 76:664, 1996.

[8] J.D. Perkins, A. Mascarenhas, Yong Zhang, J.F. Greisz, D.J. Friedman, J.M. Olson, and S.R. Kurtz. *Phys. Rev. Lett.*, 82(16):3312, 1999.

[9] P. Krispin, S.G. Spruytte, J.S. Harris, and K.H. Ploog. *J. Appl. Phys.*, 88:4153, 2000.

[10] W. Orellana and A.C. Ferraz. *Appl. Phys. Lett.*, 78:1231, 2001.

[11] X. Wu and G.C. Weatherly. *Atca. Mater.*, 47:3383, 1999.

[12] J.C. Park and B. Kang. *IEEE Trans. Plasma Sci.*, 25:1398, 1997.

[13] K. Niazi, A.J. Lichtenberg, and M.A. Lieberman. *IEEE Trans. Plasma Sci.*, 23:834, 1995.

[14] W.W. Macalpine and R.O. Schildknecht. *Proc. IRE*, 47:2099, 1959.

[15] B.J. Robinson, L. Yuan, D.A. Thompson, S.A. McMaters, and R.W. Streater. *Proc. SPIE*, 4078:18, 2000.

[16] S.M. Sze. *Semiconductor Devices, Physics and Technology*. John Wiley and Sons, New York, New York, 1985.

[17] R.A. Serway. *Physics for Scientists and Engineers*. Saunders College Publishing, Toronto, 1992.

[18] L.J. Van der Pauw. *Philips Res. Repts.*, 13:1, 1958.

[19] L.J. Van der Pauw. *Philips Tech. Rev.*, 20:220, 1958.

[20] R.K. Ahrenkiel Y.G. Hong, C.W. Tu. *J. Crystal Growth*, 227-228:536, 2001.

[21] S.R. Kurtz, A.A. Allerman, C.H. Seager, R.M. Sieg, and E.D. Jones. *Appl. Phys. Lett.*, 77:400, 2000.

[22] A. Fleck, B.J. Robinson, and D.A. Thompson. *Appl. Phys. Lett.*, 78:1694, 2001.

[23] S. Tanaka, A. Moto, M. Takahashi, T. Tanabe, and S. Takagishi. *J. Cryst. Growth*, 221:467, 2000.

[24] N.V. Joshi. *Photoconductivity: Art, Science and Technology*. Marcel Dekker, Inc, New York, New York, 1990.

[25] C. Kittel. *Introduction to Solid State Physics*. Academic Press Inc., Toronto, 1986.

[26] M. Weyers, M. Sato, and H. Ando. *Jpn. J. Appl. Phys.*, 31:L853, 1992.

[27] A.S. Jordan. *J. Appl. Phys.*, 51:2218, 1980.

[28] S.R. Johnson and T. Tiedje. *J. Appl. Phys.*, 78:5609, 1995.

[29] G.D. Cody. *J. Non-Crystalline Solids*, 141:3, 1992.

[30] K. Uesugi, I. Suemune, T. Hasegawa, T. Akutagawa, and T. Nakamura. *Appl. Phys. Lett.*, 76:1285, 2000.

[31] S.G. Spruytte, C.W. Coldren, J.S. Harris, W. Wampler, P. Krispin, K. Ploog, and M.C. Larson. *J. Appl. Phys.*, 89:4401, 2001.

[32] F. Urbach. *Phys. Rev. B*, 92:1324, 1953.

[33] S. John and C.H. Grein. *Review of Solid State Science*, 4:1, 1990.

[34] G.D. Cody. *Semiconductors and Semimetals Vol.21*. Academic Press Inc., Toronto Ont, 1984.

[35] I.A. Buyanova, W.M. Chen, B. Monemar, H.P. Xin, and C.W. Tu. *Appl. Phys. Lett.*, 75:3781, 1999.

[36] R.A. Mair, J.Y. Lin, H.X. Jiang, E.D. Jones, A.A. Allerman, and S.R. Kurtz. *Appl. Phys. Lett.*, 76:188, 1953.

[37] H.A. McKay, R.M. Feenstra, T. Schmidtling, and U.W. Pohl. *Appl. Phys. Lett*, 78:82, 2000.

[38] H.A. McKay, R.M. Feenstra, T. Schmidtling, U.W. Pohl, and J. F. Geisz. *J. Vac. Sci. Technol. B*, 19:1644, 2001.

[39] P. Krispin, S.G. Spruytte, J.S. Harris, and K.H. Ploog. *J. Appl. Phys.*, 89:6294, 2001.

[40] F. Abulfotuh, A. Balcioglu, D. Friedman, J. Geisz, and S. Kurtz. *AIP Proc.*, 464:492, 1999.

[41] D. Kwon, R.J. Kaplar, S.A. Ringel, A.A. Allerman, S.R. Kurtz, and E.D. Jones. *Appl. Phys. Lett.*, 74:2830, 1999.

[42] P. Krispin, S.G. Spruytte, J.S. Harris, and K.H. Ploog. *J. Appl. Phys.*, 88:4153, 2000.

[43] Z.G. Wang, L.A. Ledebo, and H.G. Grimmeiss. *J. Phys. C.*, 17:259, 1984.

[44] Martin Adamcyk. *Private Communication.*

[45] E.V.K. Rao, A. Ougazzaden, Y. Le Bellego, and M. Juhel. *Appl. Phys. Letters*, 72:1409, 1998.

[46] R.S. Popovic. *Hall Effect Devices: Magnetic Sensors and Characterization of Semiconductors.* A. Hilger, Bristol, England, 1991.

Appendix A

Contact Formation

The details of ohmic contacts have been discussed in section 2.5, however it is also important to note different methods and metal contacts that did not work. For example, it is essential that all samples be etched in an HCl solution to remove any oxide buildup; five minutes is enough.

Variations in the anneal time and annealing temperature have been investigated. The contacts still display ohmic characteristics whether the contacts are annealed at 500°C or 550°C, or for 20, 30 or 40 seconds.

For n-type samples, it is common to use only indium for contacts. It was observed that the contacts did not anneal properly and they were not ohmic. For p-type samples, Ti-Pt-Au contacts are commonly used, however Ti-Au contacts were tried due to the difficulty in evaporating Pt. For Pt, the emission current in the electron beam evaporator had to be ramped up very slowly and low growth rates (<0.5 Å/s) had to be used. The danger in increasing the emission current too quickly is that trapped gas in the source will heat too

Metal	Growth Rate	Emission Current	Variac	Thickness p-type	Thickness n-type
Indium	2-3 Å/s	-	55-60%	-	1500 Å
Titanium	1.0 Å/s	0.04 A	-	120 Å	-
Platinum	0.4 Å/s	0.15 A	-	100 Å	-
Gold	1.5 Å/s	0.08 A	-	1000 Å	100 Å

Table A.1: Deposition conditions for electron beam and thermal evaporation

fast and escape from the source violently. This leaves craters in the charge which result in uneven heat distribution and evaporation. The Ti-Au contacts were not ohmic.

A.1   Contact Deposition Conditions

The following steps outline the conditions used during deposition. The base pressure should be less than 2×10^{-6} Torr. When evaporating, the pressure should rise no higher than 5×10^{-6} Torr. For electron beam evaporation, the emission current should be ramped slowly, approximately 0.005 A every 30 seconds until the optimum growth rate is reached. Table A.1 lists the growth conditions during evaporation of indium, gold, titanium and platinum. The samples were not heated during contact deposition.

Appendix B

Form Factor

A form factor correction term is used in the calculations for the resistivity when doing Hall measurements. It is a geometric correction due to the method in which the voltages are measured. Using the experimental setup discussed in section 3, the resistivity can be calculated using

$$\rho = \frac{\pi}{4\ln 2} \frac{t}{I} f \left(V_{12,34} - V_{21,34} + V_{23,14} - V_{32,41} \right) \tag{B.1}$$

where t is the sample thickness, I is the applied current, $V_{12,34}$ is the voltage measured between contacts 3 and 4 when current is applied from contact 1 to contact 2, and f is the form factor. The ratio of the voltage measured between the first two contacts (3,4) and the other two contacts (1,4) is Q, defined as

$$Q = \frac{V_{12,34} - V_{21,34}}{V_{23,14} - V_{32,41}} \tag{B.2}$$

If Q is less than unity, the reciprocal is taken so that Q is always greater than one.

The form factor can then be numerically solved using[46]

$$\frac{Q-1}{Q+1} = \frac{f}{\ln 2}\,\text{arccosh}\left[\frac{1}{2}\exp\left(\frac{\ln 2}{f}\right)\right] \tag{B.3}$$

The form factor is typically very close to 1.